AAC
Journals.ASM.org

Effect of Suberoylanilide Hydroxamic Acid (SAHA) Administration on the Residual Virus Pool in a Model of Combination Antiretroviral Therapy-Mediated Suppression in SIVmac239-Infected Indian Rhesus Macaques

Gregory Q. Del Prete,[a] Rebecca Shoemaker,[a] Kelli Oswald,[a] Abigail Lara,[a] Charles M. Trubey,[a] Randy Fast,[a] Douglas K. Schneider,[a] Rebecca Kiser,[a] Vicky Coalter,[a] Adam Wiles,[a] Rodney Wiles,[a] Brandi Freemire,[a] Brandon F. Keele,[a] Jacob D. Estes,[a] Octavio A. Quiñones,[c] Jeremy Smedley,[b]* Rhonda Macallister,[b] Rosa I. Sanchez,[d] John S. Wai,[d] Christopher M. Tan,[e] W. Gregory Alvord,[c] Daria J. Hazuda,[d] Michael Piatak, Jr.,[a] Jeffrey D. Lifson[a]

AIDS and Cancer Virus Program[a] and Laboratory Animal Sciences Program,[b] Leidos Biomedical Research, Inc., Frederick National Laboratory for Cancer Research, Frederick, Maryland, USA; Statistical Consulting, Data Management Services, Inc., Frederick, Maryland, USA[c]; Merck Research Labs, West Point, Pennsylvania,[d] and Kenilworth, New Jersey,[e] USA

Nonhuman primate models are needed for evaluations of proposed strategies targeting residual virus that persists in HIV-1-infected individuals receiving suppressive combination antiretroviral therapy (cART). However, relevant nonhuman primate (NHP) models of cART-mediated suppression have proven challenging to develop. We used a novel three-class, six-drug cART regimen to achieve durable 4.0- to 5.5-log reductions in plasma viremia levels and declines in cell-associated viral RNA and DNA in blood and tissues of simian immunodeficiency virus SIVmac239-infected Indian-origin rhesus macaques, then evaluated the impact of treatment with the histone deacetylase inhibitor (HDACi) suberoylanilide hydroxamic acid (SAHA; Vorinostat) on the residual virus pool. *Ex vivo* SAHA treatment of CD4$^+$ T cells obtained from cART-suppressed animals increased histone acetylation and viral RNA levels in culture supernatants. cART-suppressed animals each received 84 total doses of oral SAHA. We observed SAHA dose-dependent increases in acetylated histones with evidence for sustained modulation as well as refractoriness following prolonged administration. *In vivo* virologic activity was demonstrated based on the ratio of viral RNA to viral DNA in peripheral blood mononuclear cells, a presumptive measure of viral transcription, which significantly increased in SAHA-treated animals. However, residual virus was readily detected at the end of treatment, suggesting that SAHA alone may be insufficient for viral eradication in the setting of suppressive cART. The effects observed were similar to emerging data for repeat-dose SAHA treatment of HIV-infected individuals on cART, demonstrating the feasibility, utility, and relevance of NHP models of cART-mediated suppression for *in vivo* assessments of AIDS virus functional cure/eradication approaches.

Although combination antiretroviral therapy (cART) can result in suppression, and perhaps the complete cessation, of measurable active HIV replication in treated patients, recrudescent virus can rebound upon treatment interruption, even in well-suppressed patients after many years of treatment (1, 2). The inability of cART to clear HIV infection is due, at least in part, to the existence of a durable residual virus pool, including latent virus, that can persist in treated patients and reinitiate active infection upon treatment cessation (3–6). As a result, lifelong treatment with antiretroviral drugs is required in the vast majority of HIV patients. In addition to concerns about the potential emergence of drug-resistant viral variants, there are considerable financial costs and concerns for drug toxicities for such long-term treatment. Recent studies have also shown increased morbidities and reduced life expectancies in association with elevated biomarkers of immune activation in well-suppressed patients compared with uninfected individuals (7–17). Thus, there is an imperative to identify definitive treatments of HIV infection that result in either the complete eradication of virus or durable control of residual viral replication in the absence of cART.

While the exact magnitude and nature of the cellular reservoirs harboring residual virus *in vivo* that provide the source of recrudescent virus when cART is stopped have not been completely elucidated, at least part of the residual virus pool consists of latently infected resting CD4$^+$ T cells, which harbor integrated proviral DNA but do not actively produce virus (3, 5, 18). Other cellular and anatomical sources for residual virus have also been suggested, including macrophages, cells in the central nervous system, and hematopoietic progenitor cells (19–22), as well as persistent low-level viral replication due to incomplete suppression in tissues (23). A number of potential mechanisms that may contribute to the lack of virus production from latently infected cells, including pre- and postintegration mechanisms and transcriptional and translational latency, have been demonstrated in various *in vitro* and *ex vivo* systems (reviewed in references 24 and 25). Numerous aspects of the transcriptional environment of resting CD4$^+$ T cells have been proposed as potential contributors to

Received 27 June 2014 Returned for modification 29 July 2014
Accepted 25 August 2014
Published ahead of print 2 September 2014
Address correspondence to Jeffrey D. Lifson, lifsonj@mail.nih.gov.
* Present address: Jeremy Smedley, Division of Primate Resources, Washington National Primate Research Center, Seattle, Washington, USA.

doi:10.1128/AAC.03746-14

transcriptional silencing of integrated proviruses. In addition to the sequestration and nuclear exclusion of critical transcription factors, the recruitment of histone deacetylases (HDACs) to the viral long terminal repeat (LTR) region and the resulting reduced chromatin accessibility also represent a mechanism whereby viral expression is inhibited and latent infection is maintained (reviewed in reference 26). Indeed, *ex vivo* treatment of $CD4^+$ T cells from cART-suppressed patients with histone deacetylase inhibitors (HDACi) has resulted in increased levels of histone acetylation and associated expression of intracellular viral RNA (vRNA) and the production of virions (27–32). These findings were the impetus for the recent clinical evaluations in cART-suppressed subjects of a single dose and multiple doses of suberoylanilide hydroxamic acid (SAHA; Vorinostat), an HDACi approved for the treatment of cutaneous T cell lymphoma (30, 33). By inducing viral expression in latently infected cells in the presence of cART, it is hoped that these otherwise-long-lived viral reservoirs will die by lytic viral mechanisms or by host immune clearance, although recent studies have suggested that this may not occur in the absence of additional interventions (34). While a single dose of SAHA perturbed the residual virus pool in suppressed patients, measured as an increase in cell-associated viral RNA in resting $CD4^+$ T cells, this virologic effect was limited and transient (30), raising the possibility that more extensive dosing might confer a greater and/or more prolonged virologic response. However, a follow-up study that evaluated multiple-dose SAHA administration showed less consistent and lower-magnitude virologic effects after numerous SAHA treatments, suggesting that the dosing strategy may be critical for perturbing viral reservoirs via HDACi (33).

Given potential concerns over the safety, tolerability, and activity of many strategies designed to purge the residual viral pool, including multiple SAHA administrations, as well as the remaining unanswered questions regarding the nature and identity of the sources of residual virus *in vivo* and the fate of reactivated latent proviruses, animal models of combination antiretroviral drug-mediated suppression of pathogenic lentiviral replication will be critical. A number of nonhuman primate (NHP) models of lentiviral infection comprising different NHP species and different challenge viruses have been adapted for studies of cART-mediated suppression of viral replication (reviewed in reference 35). Although infection of Indian-origin rhesus macaques with the pathogenic simian immunodeficiency viruses (SIVmac239 and SIVmac251) recapitulates numerous key aspects of human HIV-1 infection and pathogenesis, including sustained, high levels of viral replication, early and profound destruction of $CD4^+$ T cells in gut-associated lymphoid tissues (GALT), the establishment of chronic immune activation, progressive loss of $CD4^+$ T cells in blood, and opportunistic infections and neoplasms (36), these models have thus far been underutilized for studies of cART, due in part to the challenges of achieving clinically relevant levels of viral suppression.

We thus sought to develop a model of durable cART-mediated suppression in Indian-origin rhesus macaques infected with SIVmac239 (to avoid potential variability and inconsistencies between different stocks of uncloned viral isolates such as SIVmac251 (37–40) without a requirement to preselect animals for atypically low pretreatment viral loads. Here, we describe a novel model of cART suppression using a three class, six drug regimen administered to a cohort of six animals beginning at 4 weeks postinfection. Using this model, we demonstrate pharmacodynamic and virologic activity for *ex vivo* SAHA treatment of rhesus macaque cells from SIV-infected cART-suppressed animals and longitudinally evaluate the pharmacodynamic and virologic effects of multiple dose SAHA treatment in the setting of suppressive cART *in vivo* by administering each animal 84 total doses of SAHA separated into four 21 day courses of daily treatment, with intervening off-SAHA rest phases. The cART and SAHA treatments were well tolerated, and SAHA treatment was associated with increases in histone acetylation and SIV RNA/SIV DNA (transcriptional ratio), indicative of *in vivo* activity. However, *in vivo* viral RNA and DNA and *ex vivo* inducible viral RNA could still be detected for all animals after 84 doses of SAHA, suggesting that additional complementary treatment approaches may be required to achieve a definitive virologic outcome. Nevertheless, similarities with emerging clinical results (33, 41), including modulation of acetylated histone levels and perturbation of the residual virus pool in treated animals, suggest the relevance of this NHP model approach and demonstrate the feasibility and utility of NHP models for studying AIDS virus reservoirs and evaluating the safety and effectiveness of a clinically relevant eradication strategy.

MATERIALS AND METHODS

Animals, virus inoculations, and drug treatments. All rhesus macaques (*Macaca mulatta*) were housed and cared for in accordance with the Association for the Assessment and Accreditation of Laboratory Animal Care (AAALAC) standards in AAALAC-accredited facilities. For SAHA pharmacokinetic studies, animals were treated according to a protocol approved by the Institutional Animal Care and Use Committee (IACUC) of Merck Research Laboratories. Two fully chair-trained, naive rhesus macaque monkeys (designated RM1 and RM2) were fasted overnight (16 to 18 h) prior to SAHA administration. Monkeys were then provided SAHA (Merck) in a food treat (45 mg/kg of body weight) in their home cages and continually observed and monitored for food consumption. Each monkey was then removed from its cage by using the pole-and-collar technique and placed in a restraint chair. Whole-blood samples were collected from the saphenous vein into tubes containing EDTA at the following time points: 0 h, 0.25 h, 0.5 h, 1 h, 2 h, 4 h, 6 h, 8 h, and 24 h following SAHA administration. The samples at the time points 0 h, 0.25 h, 0.5 h, and 1 h were collected while the monkey was restrained in the chair, while subsequent blood collections were performed by restraining the animal with the pole-and-collar technique and collecting samples through the cage door. For studies using SIV-infected animals, six rhesus macaques of Indian origin (designated DC1G, DCCP, DCEA, DCEW, DCLJ, and DCT2) were treated according to a protocol approved by the IACUC of the National Cancer Institute. At the start of the study, all animals were free of cercopithicine herpesvirus 1, SIV, simian type-D retrovirus, and simian T-lymphotropic virus type 1. Animals were each intravenously (i.v.) inoculated via the saphenous vein with SIVmac239 (1 ng p27; 4/6/07 stock; kindly provided by Ronald Desrosiers). Beginning at 4 weeks post-SIV inoculation, each animal received a cART regimen comprising the reverse transcriptase inhibitors (*R*)-9-(2-phosphonylmethoxyypropyl) adenine (PMPA; tenofovir; 20 mg/kg; Gilead Biosciences) and beta-2′,3′dideoxy-3′-thia-5-fluorocytindine (FTC; emtricitabine; 40 mg/kg; Gilead Biosciences) by once-daily subcutaneous injection, the integrase inhibitors L-870812 (‘812; 20 mg/kg; Merck) and L-900564 (‘564; 10 mg/kg; Merck), each given via the oral route twice daily, and the protease inhibitors darunavir (DRV; 600 mg; Janssen Therapeutics, purchased from the NIH pharmacy) and ritonavir (RTV; 100 mg; AbbVie, purchased from the NIH pharmacy), each also given via the oral route twice daily. Each animal received this cART regimen for 52 to 54 total weeks. Beginning at 26 to 28 weeks post-cART initiation (30 to 32 weeks postinfec-

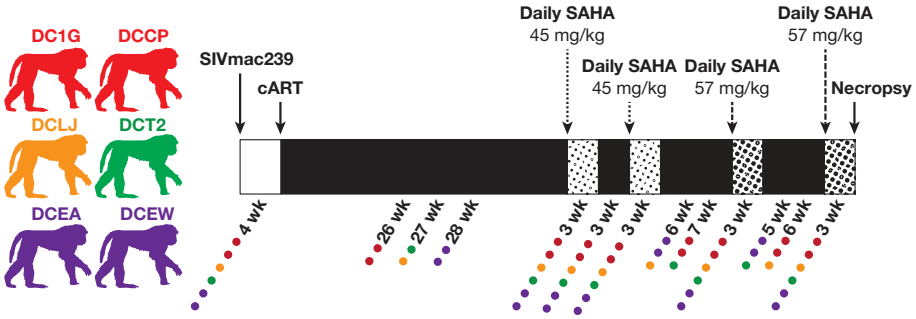

FIG 1 Schematic of the study design, with the duration of each study phase indicated. Black regions of the diagram represent study phases in which the animals were on cART; stippled regions represent study phases in which animals were on cART plus SAHA administered at the dose indicated. Due to the use of a staggered design dosing schedule, the durations of the pre-SAHA cART treatment phase and the intervening off-SAHA rest phases varied by 1 to 2 weeks between some animals. Colored dots are thus used to indicate the duration of each study phase for the macaque(s) represented by the corresponding colors.

tion), each animal received the first of four 21-day courses of SAHA via the oral route once daily (Fig. 1). The first course of SAHA (administered at 45 mg/kg once daily) was followed by a 21-day off-SAHA rest phase, a second 21-day course of oral SAHA at 45 mg/kg once daily, and then another 6- to 7-week off-SAHA rest phase. The SAHA dose was then increased to 57 mg/kg, given via the oral route once daily for 21 days, followed by a 5- to 6-week off-SAHA rest, and a final 21-day course of oral SAHA, again given at 57 mg/kg daily. Over the course of the study, each animal received 84 total doses of SAHA with concomitant cART. Safety monitoring included complete blood counts (CBC) and serum chemistry panels during cART administration.

Sample collection and preparation. Whole blood was collected from SIV-infected animals sedated with ketamine. For each SAHA course, after receiving the 7th, 14th, and 21st SAHA dose in food/treats, animals were observed for dose consumption and then sedated 2 or 4 h later for the 45-mg/kg or 57-mg/kg doses, respectively. For surgical lymph node extraction and collection of upper and lower intestinal biopsy samples during the pre-SAHA phase of the study and following the 21st dose of each SAHA course during the SAHA phase of the study, animals were sedated with ketamine and isoflurane gas for sample collection and endoscopic visualization of the upper gastrointestinal tract. Endoscopic duodenal pinch biopsy specimens and rectal pinch biopsy specimens were obtained using biopsy forceps under endoscopic and direct visualization, respectively. Plasma for viral RNA quantification and SAHA concentration determination and peripheral blood mononuclear cells (PBMC) for cell-associated viral RNA and DNA quantification, flow cytometry assays, and *ex vivo* drug treatment experiments were prepared from blood collected in EDTA Vacutainer tubes (BD). During the SAHA treatment portion of the study, whole blood collected in EDTA Vacutainer tubes was immediately placed on ice and maintained at 4°C throughout processing to prevent any changes in histone acetylation during blood transport and PBMC extraction. Following separation from whole EDTA blood by centrifugation, plasma aliquots were stored at −80°C. PBMC were isolated from whole EDTA blood by Ficoll-Paque Plus (GE Healthcare) gradient centrifugation. Lymph node mononuclear cells (LNMC) for cell-associated viral RNA/DNA quantification and spleen-derived mononuclear cells for viral outgrowth assays were prepared by mincing tissues in RPMI supplemented with 10% fetal bovine serum, and then passing the cell/medium slurry through a 70-μm cell strainer (BD). Mononuclear cell preparations of intestinal biopsy and necropsy tissues were obtained by mechanical disruption and enzymatic dissociation followed by lymphocyte separation by centrifugation through Ficoll-Paque Plus (Amersham BioScience), essentially as described previously (42). Freshly isolated PBMC were utilized for all flow cytometry-based assays. Portions of isolated PBMC and tissue-derived mononuclear cells were either viably cryopreserved or, for cell-associated viral load analyses, pelleted in a microcentrifuge and all liquid was removed prior to storage at −80°C.

Plasma viral load determinations. For plasma viral load determinations, previously frozen plasma samples were thawed and diluted 50% (vol/vol) with Tris-buffered saline (Sigma) in 1.5-ml polypropylene microcentrifuge tubes, and the virions were concentrated by pelleting at 21,000 × *g* for 1 h at 5°C. The supernatants were then removed by repeat pipetting, ensuring that the pelleted materials were not disturbed and that no more than ~5 μl of fluid remained. Each pellet was then suspended in 50 μl lysis/digestion solution (3 M guanidine-HCl [GuHCl], 50 mM Tris-Cl [pH 7.6], 1 mM $CaCl_2$, and 1 mg/ml proteinase K) and incubated at 42°C for 1 h with vortex mixing after approximately 5 and 15 min. Two hundred microliters of GuSCN/carrier solution (~5.7 M GuSCN, 50 mM Tris-Cl [pH 7.6], 1 mM EDTA, 600 μg/ml glycogen) was then added, and the sample was mixed well and allowed to incubate at room temperature for 5 min. Protein-free RNA was then recovered by the addition of 250 μl isopropanol and mixed well, and the precipitated material was collected by centrifugation at 21,000 × *g* for 10 min at room temperature. Pellets were then washed by suspension in 70% ethanol and collected by centrifugation as above, and all ethanol was removed carefully with the aid of micropipettes. The final RNA/glycogen pellets were dissolved in 30 μl 10 mM Tris-Cl, pH 8.0, for assay.

Copy number equivalents of genomic SIV RNA were determined in a two-step real-time quantitative reverse transcriptase PCR (qRT-PCR) assay as follows. cDNA was first prepared in duplicate reaction mixtures for each RNA sample in a 96-well PCR plate format. Control *in vitro* transcripts from the gag region of SIVmac239 were included to generate a reference standard curve (43). Reaction mixtures contained 10 μl RNA and 20 μl of a reverse transcription cocktail such that the final reaction mixtures contained 50 mM Tris-Cl (pH 8.3) and 50 mM KCl (1× PCR II buffer; ThermoFisher/AppliedBiosystems), 0.02% (vol/vol) Tween 20 (Sigma), 5 mM $MgCl_2$, 0.5 mM each deoxynucleoside triphosphate (dNTP), 1 mM dithiothreitol (DTT), 150 ng random hexamer primers (Roche Biochemicals), 10 U RNase inhibitor (such as RNAsin; Promega), and 40 U recombinant Moloney murine leukemia virus reverse transcriptase (Promega). Viral RNA was then converted to cDNA and prepared for real-time PCR under the following thermal profile: 25°C for 15 min, 37°C for 60 min, 90°C for 15 min, 25°C for 30 min, and 5°C hold. Upon reaching the second 25°C step for at least 2 min, the reaction plate was unsealed and 20 μl of a real-time PCR cocktail was added to each well such that final reaction mixtures contained 1× PCR II buffer, 0.012% (vol/vol) Tween 20, 4.5 mM $MgCl_2$, 600 μM dUTP, 600 nM each amplification primer and 100 nM probe (44), 45 nM SuperROX (Biosearch Technologies) as passive reference, and 1.25 U TaqGold polymerase (ThermoFisher/AppliedBiosystems). Real-time PCR and data assimilation were performed utilizing a 7500 sequence detection system (ThermoFisher/Applied Biosystems) under the following thermal profile: 95°C for 10 min to activate polymerase, followed by 45 cycles of 95°C for 15 s and 60°C for 1 min.

Ultrasensitive viral load determinations. Ultrasensitive plasma viral load determinations were accomplished essentially by increasing the amount of plasma from which virus was concentrated. Samples with volumes in the range of 1 to 5 ml were processed for RNA isolation using chemistry conditions and methods analogous to those referenced above. Virus was pelleted by ultracentrifugation at 170,000 × *g* for 30 min in a Sorvall T1270 rotor. As the co-concentration of greater amounts of nonvirus materials in the plasma was expected, with potential to interfere with accurate quantitation, we first added a known amount of RCAS virus (45, 46), nominally 1,000 copies of genomic RNA equivalents, to each sample prior to centrifugation to serve as a coassayed internal control to monitor the overall efficiency of assay performance. RNA was isolated as described above with modifications to the amounts of extraction reagents to accommodate the increased amounts of material. In brief, pellets were suspended in 100 μl lysis/digestion solution; 400 μl of GuSCN/carrier solution (modified to contain 440 μg/ml glycogen) was added followed by 500 μl isopropanol to precipitate the RNA. The final RNA/glycogen pellets were dissolved in 35 μl 10 mM Tris-Cl, pH 8.0. SIV copy number equivalents were determined in a duplex assay format with coamplification of RCAS. Assay conditions were optimized for coamplification of SIV and RCAS target sequences such that there was no cross-interference of amplifications and potential for misquantification of SIV RNA (U.S. patent application 5,705,366). cDNA was first prepared in triplicate reaction mixtures for each RNA sample in a 96-well PCR plate. Reaction mixtures contained 10 μl RNA and 20 μl cocktail, such that final reaction mixtures contained 50 mM Tris-Cl (pH 8.3), and 50 mM KCl (1× PCR II buffer; ThermoFisher/AppliedBiosystems), 0.02% (vol/vol) Tween 20 (Sigma), 5 mM $MgCl_2$, 0.5 mM each dNTP, 1 mM DTT, 150 ng random hexamer primers (Roche), 20 U RNase inhibitor (such as RNAsin [Promega]), and 20 U SuperScript II (ThermoFisher/Invitrogen). cDNA was then synthesized under the following thermal conditions: 25°C for 15 min, 42°C for 40 min, 90°C for 15 min, 25°C for 30 min, and 5°C hold. After reaching the second 25°C step for at least 2 min, the reaction plate was unsealed, and 20 μl of a real-time PCR cocktail prepared in 60 mM Tris-Cl (pH 8.5), 5 mM $MgCl_2$, and containing priming/hybridization enhancement agents, primers, probes, and passive reference at the following final reaction mixture concentrations: 6% (wt/vol) polyethylene glycol 8000 (Sigma), 15 mM $(NH_4)_2SO_4$, 600 μM dUTP, 200 nM each SIV primers SGAG21 and SGAG22, 200 nM each RCAS primers 1849F and 1869R, 100 nM SIV probe 6-carboxyfluorescein–SGAG23, 100 nM RCAS probe 5′-CalFluor-Red610-TGGGTCGGGTGGTCGTGCC-black hole quencher 2, 50 nM passive reference Quasar670-dT10–C3 blocked, and 2.5 U HotStar *Taq* polymerase (Qiagen). Real-time PCR and data assimilation were performed utilizing a 7500 sequence detection system (ThermoFisher/Applied Biosystems) under the following thermal profile: 95°C for 15 min to activate polymerase, followed by 45 cycles of 95°C for 15 s, 55°C for 1 s, and 60°C for 1 min.

Cell-associated viral load determinations. A hybrid real-time/digital PCR format and analysis approach, initially detailed by Hansen et al. (47), was applied for ultrasensitive determination of cell-associated viral loads in isolated PBMC and in mononuclear cells isolated from lymph nodes and upper and lower intestinal tissues that had been previously frozen at −80°C. For processing, all samples were maintained on dry ice to preserve nucleic acid integrity and individually were removed and rapidly disrupted in lysis/digestion solution to stabilize RNA and DNA. To each sample of pelleted cells, 100 μl of lysis/digestion solution was added and the pellet was quickly dispersed by sonication, utilizing a Branson 450 sonifier equipped with a high-intensity cup horn and set at 60% power amplitude (Branson Ultrasonics). Samples were sonicated for 10-s intervals until completely dispersed and fluid (no viscosity evident). After incubation at 42°C for 1 h to complete digestion of proteins, total nucleic acids were then recovered as described above by using 400 μl GuSCN/carrier solution and 500 μl isopropanol. The precipitate containing total nucleic acids was suspended in 60 μl 5 mM Tris-Cl (pH 8.0) with the aid of brief sonication (2 to 3 s), as above, to ensure that the sample was completely suspended/dissolved and uniform in concentration of nucleic acids. The samples were each split into two 30-μl aliquots, one for DNA analysis and one for RNA analysis. The aliquots for DNA analysis were heated to 100 to 110°C in a dry bath (Lab Armor) for 5 min and then quenched on ice in preparation for qPCR. To the aliquots for RNA analysis, 20 μl of a cocktail containing 2 μl (4 U) Turbo DNAse I and 2.5× Turbo DNAse I buffer (ThermoFisher/Ambion) was added, and samples were incubated at 42°C for 30 min to digest DNA. After digestion, RNA was recovered by addition of 200 μl of GuSCN solution without glycogen carrier, followed by precipitation with 250 μl isopropanol and a 70% ethanol wash, as noted above. For qPCR analysis, DNA samples were diluted to 150 μl with 5 mM Tris-Cl (pH 9.0); RNA samples were diluted to 150 μl with 5 mM Tris-Cl (pH 8.0). Methods and application of quantitative hybrid real-time/digital PCR in nested format were described previously by Hansen et al. (47). A total of 12 10-μl replicates of each DNA or RNA sample were tested, with two of the replicates containing a spike of DNA or RNA standard, as appropriate, to monitor assay performance and to guide retest requirements. Determined SIV DNA and RNA values were normalized to cell equivalents (CE), determined from coamplification of a target sequence in the rhesus CCR5 gene sequence as described.

***Ex vivo* viral RNA induction assays.** For samples collected prior to *in vivo* SAHA administration, viably cryopreserved PBMC from two cART-suppressed animals collected at four different bleed time points between 20 and 25 weeks post-cART initiation were thawed and pooled for each animal, and then $CD4^+$ T cells were enriched by negative selection using the $CD4^+$ T cell isolation kit for NHP (Miltenyi Biotec). Enriched $CD4^+$ T cells were then cultured in the presence of 1 μM FTC and 200 nM ‘812 and treated with either dimethyl sulfoxide (DMSO), 1 μM SAHA, 5 μM SAHA, or rhesus-specific anti-CD2/CD3/CD28-conjugated beads (Miltenyi Biotec) at 2.1×10^7 to 2.3×10^7 cells per condition. Fresh FTC and ‘812 were added back to the cultures at day 3. Viral RNA levels in frozen cell-free culture supernatants collected at days 3 and 6 were determined by first isolating RNA as described above for plasma viral load determinations. Total RNA was then suspended in 90 μl 5 mM Tris-Cl (pH 8.0). SIV RNA copy numbers were determined in a 12-replicate test format, in 384-well plates, in which the lower limit of detection was based on positive amplification of sample in 1 out of 12 replicates. cDNA was first prepared in a 15-μl reaction mixture that contained 5 μl sample and 10 μl of a reverse transcriptase cocktail at the final concentrations described above but containing 20 U SuperScript II reverse transcriptase (ThermoFisher/Invitrogen) per reaction mixture. These reaction mixtures were then supplemented with 10 μl of real-time PCR cocktail containing primers, probe, and *Taq* polymerase at the final concentrations described above for plasma viral load determinations, without the additional preamp or “nested” protocol. Real-time PCR and assimilation of data were performed on a 384-well instrument, ViiA7 or QuantStudio 12K Flex, from ThermoFisher/Applied Biosystems. For samples collected at necropsy, viably cryopreserved single-cell suspensions of lymph node cells were thawed or freshly collected PBMC were used. $CD4^+$ T cells were enriched by negative selection using the $CD4^+$ T cell isolation kit for NHP (Miltenyi Biotec) and then cultured in the presence of either DMSO, 1 μM SAHA, 5 μM SAHA, or rhesus specific anti-CD2/CD3/CD28-conjugated beads (Miltenyi Biotec). Viral RNA in frozen cell-free culture supernatants collected at 48 h was isolated and detected/quantified.

LC-MS quantitative assay of SAHA plasma concentrations. The concentrations of SAHA in plasma were determined by tandem liquid chromatography-mass spectrometry (LC-MS) assays following a protein precipitation step. Aliquots of plasma were precipitated by addition of acetonitrile containing an internal standard (labetalol or penta-deuterated SAHA), followed by vortexing and centrifugation. An aliquot of the supernatant was diluted with an equal volume of water and injected for analysis. Separation of SAHA was achieved on a C_{18} column using a mobile phase consisting of 0.1% formic acid in water (solvent A) and 0.1% formic acid in acetonitrile (solvent B). The chromatography was run using

a step gradient from a high percentage of solvent A to a high percentage of solvent B and equilibrating back to the original percentage of solvent A. Quantification was performed by monitoring the transition of *m/z* 265.3 to *m/z* 93.9 or 232.2 for SAHA and *m/z* 329.2 to *m/z* 162.1 for labetalol or 270.2 to 237.2 for penta-deuterated SAHA. The linear method afforded a lower limit of quantitation between 1 and 4 nM.

Flow cytometry. Antibodies and reagents for flow cytometry were obtained from BD Biosciences, unless indicated otherwise, and data analysis was performed using FCS Express software (De Novo Software). Absolute cell counting was performed on EDTA-anticoagulated whole blood as previously described (48, 49), using the following immunophenotyping panel: CD45-fluorescein isothiocyanate (FITC; DO58-1283), CD3-phycoerythrin (PE; SP34-2), CD4-allophycocyanin (APC; L200), CD14-APC-Cy7 (M5E2; Biolegend), CD8α PE-Cy7 (SK1), and CD20 Pacific Blue (2H7; Biolegend). Samples were lysed, and approximately 50,000 $CD45^+$ $CD3^+$ cells were acquired for each sample to calculate cell counts by using a BD FACSVerse flow cytometer equipped with a volumetric flow sensor.

Acetylated histone assay. Acetylated histone levels in PBMC following *ex vivo* and *in vivo* SAHA treatment were determined using a flow cytometric assay. Approximately 2×10^6 freshly isolated rhesus PBMC, maintained at 4°C throughout prior handling and processing from whole blood, were surface immunophenotyped for 20 min at room temperature in the dark (RTD) by using the following antibody panel: CD69-brilliant violet (BV) 421 (FN50; Biolegend), CD4–V500 (L200), CD14-BV570 (M5E2; Biolegend), CD8-PE (SK1), CD28-ECD (CD28.2; Beckman Coulter), CD95-PE-Cy5 (DX2), PD-1–PE-Cy7 (EH12.2H7; Biolegend), and CD3–APC-Cy7 (SP34-2). Cells were immediately treated with PhosFlow lyse/fix buffer and incubated for 30 min at 37°C, washed twice, permeabilized with 0.4% Triton X-100 buffer (Sigma) for 10 min at RTD, and washed again. Permeabilized cells were then stained intracellularly for 30 min at 4°C in the dark with the following antibodies: acetylated histone (recognizes several acetylated residues on histones H3 and H4; 3HHH4-2C2; Active Motif) and Ki67-FITC (B56). Prior to use, the acetylated histone antibody was FITC labeled by using a Zenon reagent kit (Invitrogen), according to the manufacturer's instructions. After washing, stabilizing fixative was added, and approximately 200,000 $CD3^+$ T cells were acquired for each sample by using a BD LSR-II flow cytometer. Population gating was performed using corresponding fluorescence minus one (FMO) and untreated negative-control samples. *In vitro* HDACi-treated, purified T cells were immunophenotyped by using the same protocol, except the following surface staining panel was used: yellow fluorescent reactive dye (to detect dead cells; Invitrogen), CD4-V500 (L200), CD69-PE (FN50; Biolegend), CD28-ECD (CD28.2; Beckman Coulter), CD95–PE-Cy5 (DX2), CD8-PE-Cy7 (SK1), and CD3–APC-Cy7 (SP34-2).

Statistical analyses. Longitudinal acetylated histone H3/H4 data and transcriptional ratio data were analyzed with a longitudinal repeated-measures analysis of variance and linear hierarchical mixed-effects models (50, 51). These models take into consideration the correlation/covariation of responses within the same animal over time. Ac-H3/H4 and SIV RNA:DNA data for six macaques were recorded for various numbers of occasions, within eight treatment cART/SAHA phases. Independent (orthogonal) variance components of the factors in the experimental setup were calculated, and appropriate variance ratios were computed to test for questions of interest, in particular, for differences among phases across time (50). Not all comparisons of interest were completely independent of others. Therefore, the potential compounding type I error rate due to multiple testing was controlled through the use of the Benjamini-Hochberg (BH) or false discovery rate (FDR) correction (52). Our reported probabilities are thus conservative (i.e., not as low as the original [raw] probabilities obtained in the analyses). Probability values less than 0.05 were considered significant.

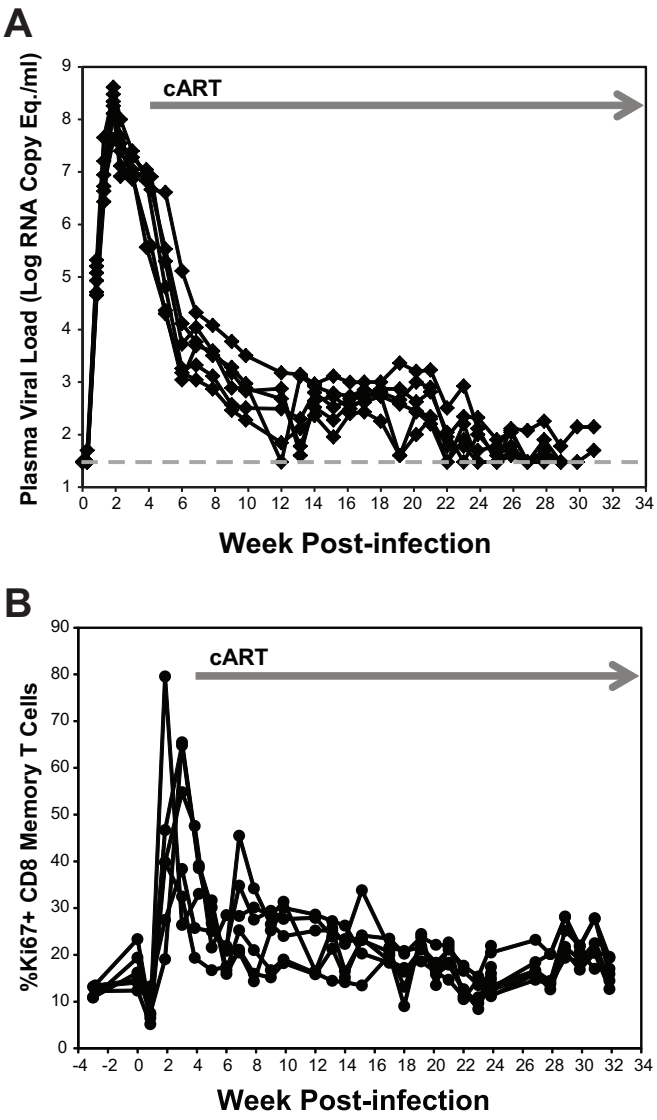

FIG 2 Virologic and immunologic responses to cART. (A) Plasma viral loads in six animals treated with cART starting at 4 weeks postinfection (gray arrow), determined via a qRT-PCR assay with a 30-copy/ml quantification limit (dashed gray line). Data for two of the six animals shown have been reported previously (35). (B) Longitudinal analysis of the percent $CD8^+$ memory T cells that are $Ki67^+$ with cART treatment (gray arrow) for the same six animals shown in panel A. Data shown in both panels A and B are for the pre-SAHA treatment phase of the study.

RESULTS

cART treatment in SIVmac239-infected animals. To develop and characterize a model of cART-mediated suppression of pathogenic SIV infection, we first intravenously inoculated six naive Indian-origin rhesus macaques (*Macaca mulatta*) with SIVmac239 (Fig. 1). Peak viremia levels in all six animals were typical of SIVmac239 infection in unvaccinated animals, ranging from 4.1×10^7 to 4.1×10^8 RNA copies/ml by 2 weeks postinfection (Fig. 2A). At 4 weeks postinfection, a six-drug cART regimen comprising two RT inhibitors (FTC and PMPA), two integrase inhibitors (L-'564 and L-'812), and one protease inhibitor (darunavir, with ritonavir provided as a boosting agent, per clinical practice) was initiated in all six animals (Fig. 1). Each animal

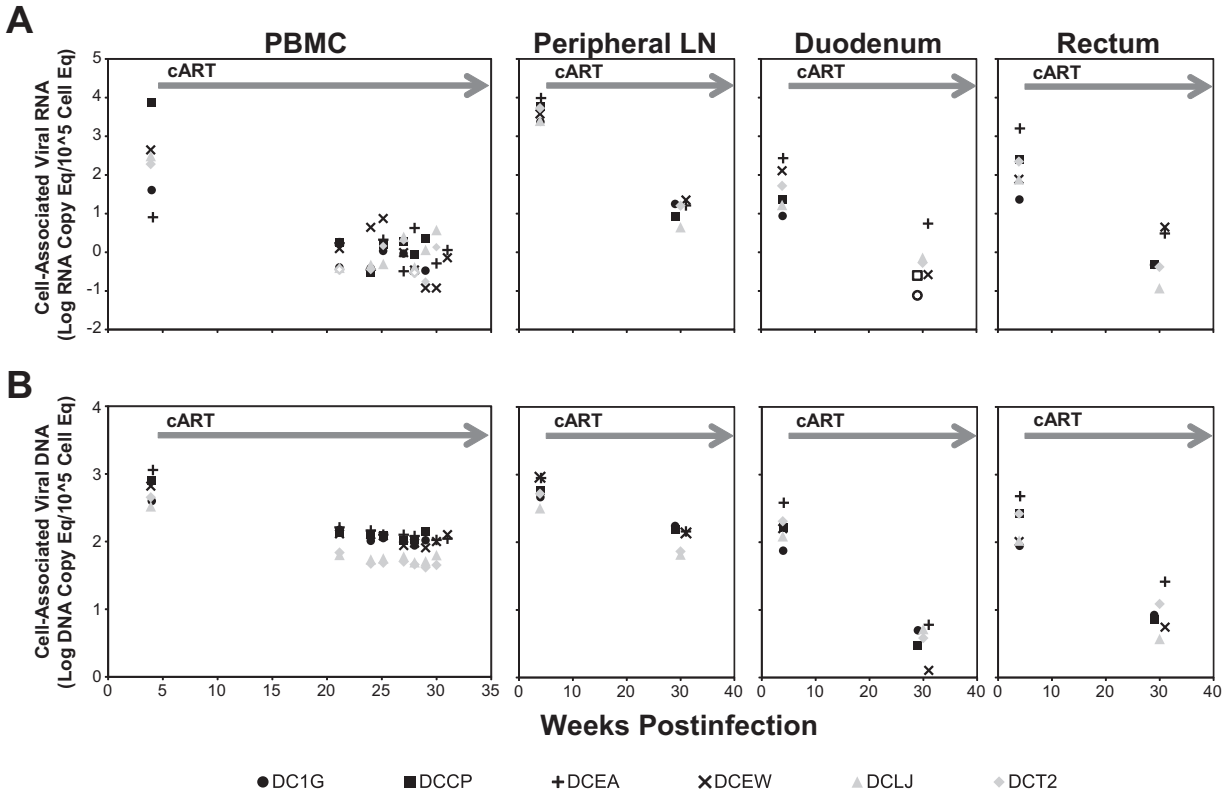

FIG 3 Cell-associated viral loads in blood and tissues from animals on cART. Cell-associated viral RNA (A) and DNA (B) levels, measured by qRT-PCR or qPCR, respectively, at the indicated time points in blood (PBMC) and tissues in cART-treated animals are shown. Results for each animal are represented by a unique plot symbol. Values were normalized based on input cell numbers, determined by independent qPCR measurements of a host cell gene. For each plot, treatment with cART is indicated by a gray arrow. Open symbols represent values below the assay quantification limits, plotted as the quantification limit normalized for input cell number. Peripheral LN, peripheral lymph node (axillary or inguinal).

received this drug regimen for 52 to 56 total weeks, including 26 to 28 weeks prior to the first administration of SAHA. The cART regimen was safe and well-tolerated in all 6 animals, with modest changes in serum creatinine and inorganic phosphorous levels measured after 10 to 12 months of treatment in three of the animals (data not shown), consistent with mild tenofovir-related renal toxicity (53). Pretreatment viral loads ranged from 3.7×10^5 to 1.1×10^7 RNA copies/ml plasma, with all six animals showing a 1.5- to 3.5-log reduction in viremia within the first 2 weeks of treatment (Fig. 2A). Thereafter, further declines in viremia were more gradual, with plasma viral loads for five of six animals dropping below the assay quantification limit (30 RNA copies/ml) at one or more sampling time points within 20 weeks on cART. By 23 weeks, the six-drug cART regimen durably suppressed viral replication in four out of six animals to clinically relevant levels (<50 RNA copies/ml) with a single 50-copy/ml viremia blip in each of two of the animals over the next 4 weeks. For the remaining two animals, plasma viral loads were suppressed to <200 and <100 RNA copies/ml within 23 weeks on cART. Overall, viremia for each of the six animals declined by approximately 4 to 5.5 logs within ~6 months on cART.

Previous studies have noted a decline in immune activation in HIV-infected humans following the initiation of effective ART (11, 54–56). Although in untreated SIV-infected macaques immune activation declines following a dramatic initial increase during the acute phase of infection, it typically remains elevated above preinfection levels during the chronic phase of infection (57). To determine if our cART regimen could normalize immune activation levels in our SIV-infected animals, we longitudinally evaluated immune activation as measured by Ki67 staining on $CD8^+$ memory T cells (Fig. 2B). Following a marked upregulation during acute infection that peaked at 2 to 3 weeks postinfection, immune activation levels declined with cART treatment, returning to essentially preinfection baseline levels within 12 to 16 weeks on cART.

We next examined the impact of our cART regimen on cell-associated viral loads in blood and in tissues relevant to SIV replication. Prior to cART initiation, there was a wide range in cell-associated viral RNA levels in PBMC between animals, ranging from 8 to 7,500 vRNA copies/10^5 CE (Fig. 3A). By 17 weeks post-cART initiation, PBMC-associated vRNA levels for all six animals declined to <8.0 vRNA copies/10^5 CE. Apart from one time point each for animals DCEA and DCLJ and two time points for DCEW, PBMC-associated vRNA measurements remained at <3.0 copies/10^5 CE for all time points for the 8 weeks preceding the initiation of SAHA treatment. In contrast to PBMC, cell-associated viral RNA levels in peripheral LN were more consistent between animals prior to cART, ranging from 2,500 to 9,700 vRNA copies/10^5 CE, with >2-log declines for all six animals after 24 to 26 weeks of cART. Declines in cell-associated vRNA levels were also measured in GALT samples taken after 6 months of cART. Upper gastrointestinal tract (duodenum) samples declined to <1.0 vRNA copy/

10^5 CE for 5 of 6 animals, with the remaining animal with the highest pretreatment cell-associated vRNA levels in the duodenum (animal DCEA) declining to 6.0 vRNA copies/10^5 CE. For the lower gastrointestinal tract (rectum), cell-associated vRNA levels similarly fell to <1.0 vRNA copy/10^5 CE for 4 of 6 animals, while animals DCEA and DCEW declined to 3.0 and 4.5 vRNA copies/10^5 CE, respectively. Overall, cell-associated vRNA levels for PBMC, peripheral LN, duodenum, and rectum showed mean declines on cART of 2.1 to 3 logs.

Although cell-associated viral DNA levels in PBMC, peripheral LNs, and GALT also declined on cART, the magnitude of reduction was smaller than for viral RNA (Fig. 3B). PBMC and LN, which had the highest pretreatment vDNA levels, demonstrated the most limited reduction in cell-associated vDNA, with 3- to 7-fold declines in all six animals following ~6 months of cART. Duodenum and rectum samples showed somewhat greater declines, with cell-associated vDNA levels declining by 1 to 2 logs for all 6 treated macaques.

SAHA administration. Treatment of latently infected cells with SAHA and other HDACi compounds has been shown to induce viral transcription and virus production in several *in vitro* models of HIV-1 latency (58–65) and in primary $CD4^+$ T cell from cART-suppressed patients (27–32). Moreover, HIV-1 cell-associated viral RNA levels in resting $CD4^+$ T cells transiently increased in cART-suppressed patients following a single oral administration of the HDACi SAHA, demonstrating the potential for SAHA to perturb viral latency *in vivo* (30). Given the potential safety concerns for repeat dosing of SAHA in HIV-1-infected patients, we sought to evaluate the effect of multiple-dose SAHA administration in our cART-suppressed SIVmac239-infected macaques. We thus began by assessing the pharmacokinetics and pharmacodynamic activity of SAHA in rhesus macaques to determine the utility of our nonhuman primate model for evaluating the impact of SAHA on SIV-infected cells. First, we performed a preliminary pharmacokinetic study in uninfected animals to define the plasma SAHA concentrations achievable with oral SAHA dosing in rhesus macaques. Two SIV-naive, Indian-origin rhesus macaques were fasted for 12 to 16 h and then given a single dose of SAHA at 45 mg of drug per kg of body weight in a food vehicle. Plasma drug concentrations showed rapid pharmacokinetics, peaking at 1.84 μM by 1 h postdose in animal RM1 and at 1.88 μM by 2 h postdose in animal RM2, but dropping to <0.3 μM in both animals by 4 h postdose (Fig. 4).

We next evaluated the pharmacodynamic activity of SAHA in inducing increases in histone acetylation and SIV production in *ex vivo*-treated primary rhesus macaque $CD4^+$ T cells obtained from our cART-suppressed animals. As shown in Fig. 5A, acetylated histone levels in blood-derived rhesus $CD4^+$ T cells showed a clear dose-dependent increase within 24 h of *ex vivo* treatment with SAHA, confirming the pharmacodynamic effect of SAHA treatment in rhesus macaque $CD4^+$ T cells. SAHA-induced increases in acetylated histone levels were also associated with a measurable increase in SIV production from infected cells obtained from cART-suppressed animals (Fig. 5B). Although low levels of vRNA accumulated by day 3 and increased slightly by day 6 in the supernatants of cells treated with the negative-control vehicle (DMSO), treatment with 1 or 5 μM SAHA induced an upregulation in vRNA over DMSO treatment in culture supernatants for both animals by day 3, with further increases in vRNA for the 5 μM SAHA treatment for both animals by day 6. Viral RNA accumulation in culture supernatants increased further by day 6 with 1 μM SAHA treatment for only one of the two animals. As expected, cell activation with anti-CD2/CD3/CD28 beads also induced an upregulation of virion production, which exceeded the amount of virus produced following either of the SAHA treatments, consistent with findings for *ex vivo* treatment of cells from cART-suppressed HIV-1-infected people (30, 66, 67).

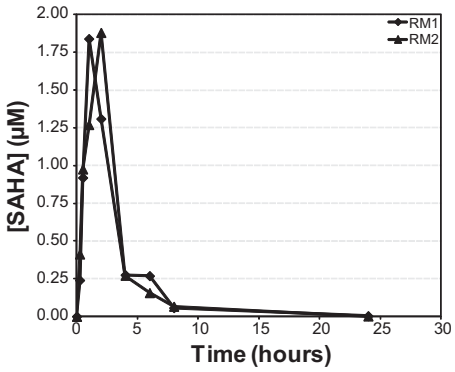

FIG 4 Pharmacokinetics of oral SAHA administration in naive animals. Plasma SAHA concentration over time is shown for two naive Indian-origin rhesus macaques (RM1 and RM2) following a single oral dose of SAHA, administered at 45 mg/kg.

Plasma viral loads with *in vivo* SAHA treatment. Having established the ability of SAHA to induce increases in acetylated histone levels and SIV production following *ex vivo* treatment of $CD4^+$ T cells taken from our cART-suppressed rhesus macaques, we next evaluated the impact of *in vivo* SAHA treatment in a multiple-dose study. As shown schematically in Fig. 1, each of the six cART-suppressed animals received 84 total doses of oral SAHA, divided into 4 courses of daily treatment, beginning at 25 to 28 weeks post-cART initiation with continued cART throughout. Building on our pharmacokinetic results and SAHA treatment regimens for cutaneous T cell lymphoma in humans, each of the four SAHA courses comprised 21 daily doses of SAHA with at least 3 weeks of off-SAHA rest between each SAHA treatment phase. Each daily dose within the first two SAHA treatment phases was administered at 45 mg/kg of body weight, matching that used in the single-dose pharmacokinetic study performed in uninfected animals (Fig. 4). For the final two treatment phases, each daily SAHA dose was increased by 28%, to 57 mg/kg. Oral administration was achieved by mixing the drug with food/treats provided to the animals, with the complete consumption of each dose confirmed by visual observation. CBC and serum chemistry panels were monitored throughout the study, and no abnormalities were noted in association with SAHA treatment (data not shown).

Plasma viral loads for the six cART-treated animals continued to show a range of suppression during the SAHA treatment portion of the study, comprising weeks 25 to 54 of cART. Macaques DCT2, DCLJ, and DC1G demonstrated the most complete suppression, with plasma viral loads below 30 copies/ml for the vast majority of time points and only 1 viral load measurement above 50 vRNA copies/ml for animal DCT2. Animals DCEW and DCCP had an intermediate level of suppression, with 4 and 8 time points revealing counts above 50 vRNA copies/ml, respectively. Macaque DCEA had the highest persistent viral loads during the SAHA treatment portion of the study, with most plasma viremia mea-

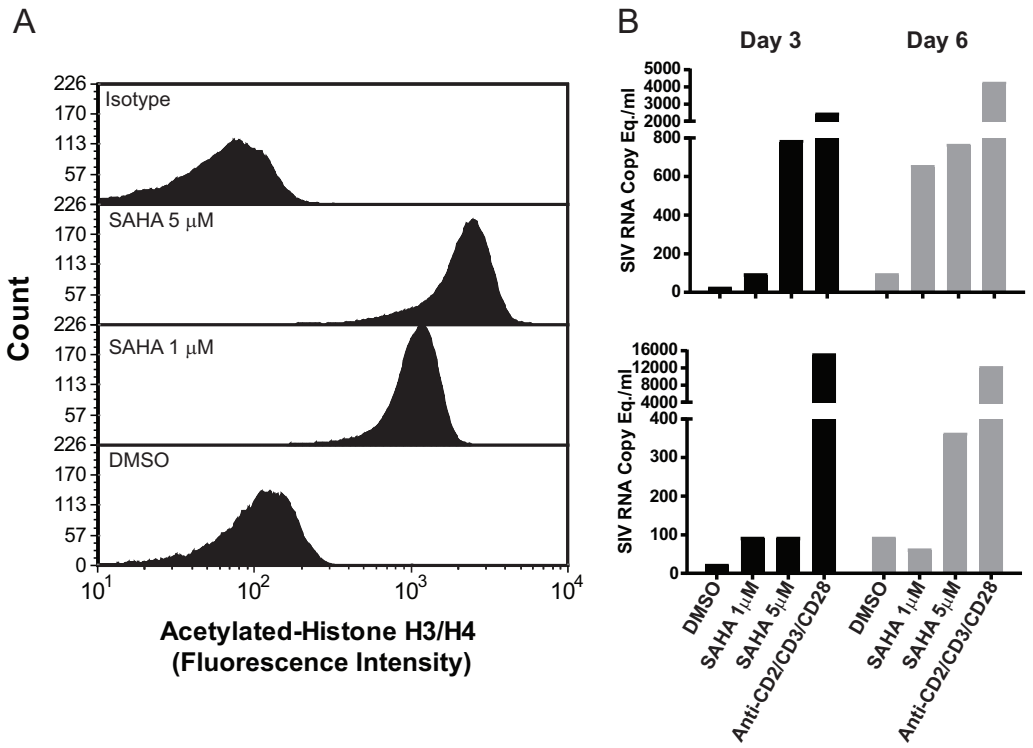

FIG 5 Changes in acetylated histone levels and virus production following *ex vivo* SAHA treatment of $CD4^+$ T cells from cART-suppressed macaques. (A) Acetylated histone H3 and H4 levels measured by flow cytometry 24 h after *ex vivo* treatment of $CD4^+$ T cells with DMSO (vehicle control) or the indicated concentrations of SAHA are shown. Results are representative data from treatment of cells from one of six cART-suppressed animals; results for other animals were highly similar. (B) Virion-associated SIV RNA in culture supernatants from two cART-suppressed macaques (top, DC1G; bottom, DCLJ) following 3 or 6 days of the indicated treatments in the presence of antiretroviral drugs.

surements above 50 vRNA copies/ml plasma and only 8 time points below 30 vRNA copies/ml (Fig. 6). Using a standard qRT-PCR assay with a 30-vRNA copy/ml quantification cutoff, viremic time points were identified for all six animals during the SAHA treatment portion of the study. However, increases in plasma viral loads were not clearly associated with the timing of SAHA treatment. It remained possible, however, that lower-magnitude viremia changes may have been induced by SAHA treatment, so select plasma viral load time points that showed <30 vRNA copies/ml by the standard assay were also assessed using an ultrasensitive method, which assayed a larger volume of plasma for greater assay sensitivity. All such samples had detectable vRNA when assessed with the ultrasensitive assay; however, there were again no clear patterns of plasma viremia increases in association with SAHA administration (Fig. 6), as was the case in clinical studies (30).

SAHA levels in cART-suppressed macaques. Based on the rapid SAHA pharmacokinetics observed in the two single-dose-treated naive macaques (Fig. 4), we evaluated plasma SAHA levels in our cART-suppressed animals at 2 h postadministration for the first two SAHA courses at 45 mg/kg. Following observed consumption of all SAHA-containing food, each animal was anesthetized and blood was collected at 2 h postadministration. Plasma SAHA levels were highly variable, both between animals and between doses for a given animal, and the levels were lower than the peak values measured during the initial pharmacokinetic study, ranging from below the limit of quantification to 0.651 μM (Table 1). At most of the post-SAHA treatment blood sampling time points, undigested food could be observed endoscopically in the treated animals' stomachs, suggesting that delayed gastric emptying may have delayed SAHA absorption. We thus reasoned that SAHA mixed into food/treats and provided to the six cART-suppressed animals *ad libitum* followed by anesthesia blood and biopsy sampling may have led to delayed pharmacokinetics relative to the fasted animals used for the single-dose pharmacokinetic study. We therefore evaluated the plasma SAHA levels at 4 h postadministration for the final two courses of SAHA at 57 mg/kg. We again observed highly variable SAHA levels, with no apparent increases in plasma SAHA concentrations, which ranged from below the limit of quantification to 0.396 μM (Table 1). Food was again observed in the stomachs of treated animals at the 4-h time point.

***In vivo* pharmacodynamic activity of SAHA: histone acetylation.** Single-dose SAHA administrations to cART-suppressed HIV-1-infected people led to transient increases in cell-associated vRNA levels in resting $CD4^+$ T cells (30), though the virologic impact following multiple SAHA doses was less clear (33). Prior to evaluating the impact of multidose SAHA treatment on SIV transcription *in vivo*, we first assessed the *in vivo* pharmacodynamic activity of SAHA in our cART-suppressed macaques. Starting just prior to the first administration of SAHA, weekly blood samples were collected and assessed by flow cytometry for acetylated histone H3 and H4 levels in $CD4^+$ T cells, as was performed on *ex vivo* SAHA-treated cells. For each 3-week SAHA course, PBMC were extracted at the end of the first, second, and third week of SAHA administration (i.e., after the 7th, 14th, and 21st dose), with

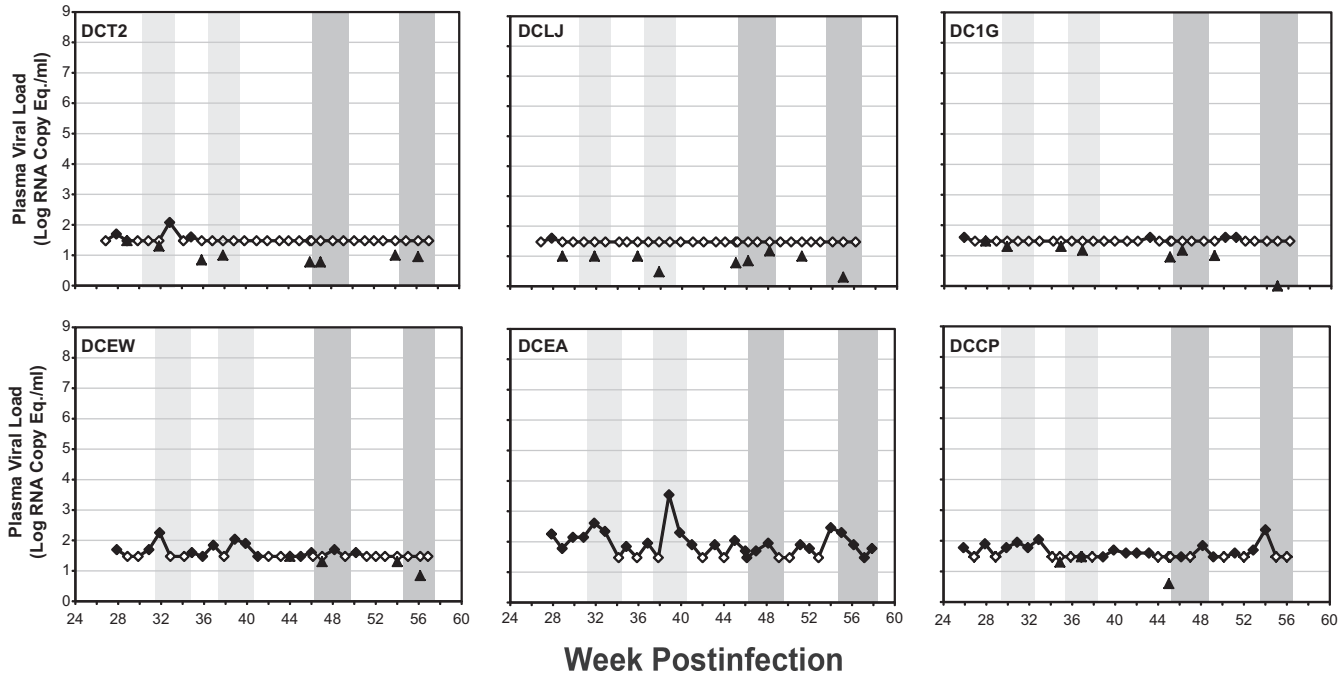

FIG 6 Plasma viral loads during the SAHA treatment portion of the study. Longitudinal plasma viral loads were measured using a qRT-PCR assay with a 30-copy/ml quantification limit (diamonds). Open symbols represent values below the assay quantification limit. Select samples were also analyzed using an ultrasensitive assay with a quantification limit determined by the volume of plasma available to assay (triangles). Light gray shaded regions indicate data for SAHA treatment at 45 mg/kg; dark gray shaded regions indicate data for SAHA treatment at 57 mg/kg. For each plot, the first four time points were replotted from Fig. 2A to show pre-SAHA baseline levels.

PBMC collection timing matched to plasma collections used for plasma SAHA concentration determinations (Table 1; i.e., 2 h postdose for the first two courses of SAHA at 45 mg/kg and 4 h postdose for the last two courses of SAHA at 57 mg/kg).

Given the highly variable plasma SAHA concentrations at the sampling time points and the complex temporal relationship between SAHA administration and pharmacodynamic activity (33), we evaluated the pharmacodynamic activity of SAHA by grouping data from time points for all six animals into eight treatment phases and then analyzed acetylated histone levels in $CD4^+$ T cells (Fig. 7). Overall, there was a highly statistically significant difference in acetylated histone levels across the eight study phases ($P < 0.0001$). Although mean Ac-H3/H4 levels were elevated in the first SAHA treatment phase (phase 2, mean Ac-H3/H4 MFI, 191) relative to the pretreatment time point (phase 1, mean Ac-H3/H4 MFI, 139), limited pretreatment data were available, and this increase was not statistically significant. Thereafter, Ac-H3/H4 levels were statistically equivalent across the first and second SAHA 45-mg/kg courses, including the intervening 3-week off-SAHA rest phase (Fig. 7, phases 2, 3, and 4; $P = 0.15$). However, during the SAHA washout phase following the second SAHA treatment phase, there was a highly significant drop in the Ac-H3/H4 levels during the lengthier 6- to 7-week off-SAHA rest phase (Fig. 7, phase 5) prior to the initiation of SAHA administration at 57 mg/kg (phases 2, 3, and 4 versus phase 5; $P < 0.0001$). This was followed by a highly significant increase in Ac-H3/H4 in the first SAHA phase at the elevated dose of 57 mg/kg (Fig. 7, phase 5 versus phase 6; $P = 0.0013$). Additionally, it is important to note that in the first SAHA phase at 57 mg/kg (phase 6), Ac-H3/H4 levels, with a mean MFI of 266, were highly significantly elevated over the earlier SAHA phases at 45 mg/kg (phases 2 and 4), with mean Ac-H3/H4 MFI values of 191 and 193, respectively ($P < 0.0001$). Starting at phase 6, there was a downward trend in the acetylated histone levels in the final three phases ($P = 0.0034$), with lower acetylated histone levels measured for the second SAHA 57-mg/kg phase (phase 8, mean Ac-H3/H4 MFI, 197) than for the preceding off-SAHA rest phase.

Cell-associated viral load changes with *in vivo* SAHA treatment. Previous studies have shown that HDACi treatment leads to an increase in viral gene transcription in latently infected cells (28, 30, 58–60). To evaluate changes in viral transcription during *in vivo* SAHA administration, we quantified cell-associated vRNA and vDNA in PBMC and calculated the ratio of these two, defined here as the viral transcriptional ratio. This approach has two advantages. First, permissible survival bleed volumes for rhesus macaques make it difficult to sort cells for sufficient yields of specific cellular subsets, such as resting $CD4^+$ T cells, in which latent viral genomes might be enriched. By comparing changes in vRNA to vDNA we effectively focused our analysis on vRNA changes only in infected cells across study time points without a need to sort for specific cell subsets. Second, by comparing vRNA to vDNA levels, we could specifically assess changes in viral gene expression, while reducing the impact of any confounding effects of SAHA treatment, such as potential mobilization of infected cells harboring vRNA from tissues into blood, which could give the artificial perception of an increased vRNA level per cell.

As was done for the acetylated histone analysis, changes in viral transcription during SAHA treatment were also evaluated by comparing treatment phases for all six animals. No changes in the

TABLE 1 Plasma SAHA levels in cART-suppressed macaques

Animal	SAHA course no.	Dosage (mg/kg)	Sampling day during 21-day SAHA treatment	Timing of sampling post-SAHA dose (h)	Plasma [SAHA] (μM)
DC1G	1		Predose		BLQ[a]
		45	7	2	0.231
		45	14	2	0.484
		45	21	2	0.644
	2	45	7	2	0.183
		45	21	2	0.039
	3		Predose		BLQ
		57	1	4	0.040
		57	14	4	0.231
		57	21	4	0.012
	4	57	8	4	0.032
		57	14	4	0.044
		57	21	4	0.201
DCEA	1		Predose		BLQ
		45	7	2	0.137
		45	14	2	0.021
		45	21	2	0.137
	2	45	7	2	BLQ
		45	14	2	BLQ
		45	21	2	0.018
	3		Predose		BLQ
		57	1	4	BLQ
		57	7	4	BLQ
		57	14	4	BLQ
		57	21	4	0.012
	4	57	7	4	0.002
		57	14	4	BLQ
		57	21	4	0.013
DCEW	1		Predose		BLQ
		45	7	2	0.651
		45	14	2	0.451
		45	21	2	0.344
	2	45	7	2	0.081
		45	14	2	0.167
		45	21	2	0.027
	3		Predose		BLQ
		57	1	4	0.012
		57	14	4	0.003
		57	21	4	0.037
	4	57	7	4	0.011
		57	14	4	0.036
		57	21	4	0.044
DCCP	1		Predose		BLQ
		45	7	2	0.087
		45	14	2	0.028
		45	21	2	0.087
	2	45	7	2	0.007
		45	21	2	0.056
	3		Predose		BLQ
		57	1	4	0.012
		57	7	4	0.011
		57	21	4	0.005
	4	57	1	4	0.007
		57	8	4	0.009
		57	21	4	0.396
DCLJ	1		Predose		BLQ
		45	7	2	0.025
		45	14	2	0.025
		45	21	2	0.248
	2	45	1	2	0.032
		45	7	2	0.185
		45	21	2	0.069
	3		Predose		BLQ
		57	1	4	0.017
		57	14	4	0.060
	4	57	1	4	0.426
		57	7	4	0.026
		57	21	4	0.027
DCT2	1		Predose		BLQ
		45	7	2	0.080
		45	14	2	0.043
		45	21	2	0.080
	2	45	7	2	0.003
		45	21	2	BLQ
	3		Predose		BLQ
		57	1	4	BLQ
		57	14	4	BLQ
	4	57	1	4	BLQ
		57	7	4	0.005
		57	21	4	BLQ

[a] BLQ, below the level of quantification (<0.002 μM).

viral transcriptional ratio were observed through the first three phases of the study (Fig. 8, phases 1, 2, and 3), encompassing pre-SAHA treatment, the first course of SAHA treatment at 45 mg/kg, and the first off-SAHA rest phase. However, in the second SAHA 45-mg/kg course, there was a statistically significant >3-fold increase in the mean viral transcriptional ratio over the preceding off-SAHA rest phase (Fig. 8, phase 3 versus phase 4; $P = 0.0092$). This elevated transcriptional ratio was maintained through the subsequent two study phases, a subsequent off-SAHA rest phase and the first SAHA phase at 57 mg/kg (Fig. 8, phases 4, 5, and 6), with significantly elevated transcriptional ratios for phases 4, 5, and 6 over phases 1, 2, and 3 ($P = 0.0019$) and over phases 7 and 8 ($P = 0.0176$). Although the viral transcriptional ratio declined in the final two study phases, which included a final off-SAHA rest phase and the final SAHA 57-mg/kg phase (Fig. 8, phases 7 and 8), they were elevated compared to phases 1, 2, and 3 ($P = 0.0167$).

At the end of the final SAHA treatment phase, animals were euthanized and blood and tissue samples were collected. For all six animals, vRNA and vDNA were readily detected in lymph node- and blood-derived cells, and viral RNA was readily detectable in culture supernatants of blood- and lymph node-derived $CD4^+$ T cells cultured *ex vivo* in the presence of SAHA and/or activating stimuli (data not shown), demonstrating that repeated administrations of SAHA in the setting of suppressive cART did not result in the eradication of inducible virus from the treated animals.

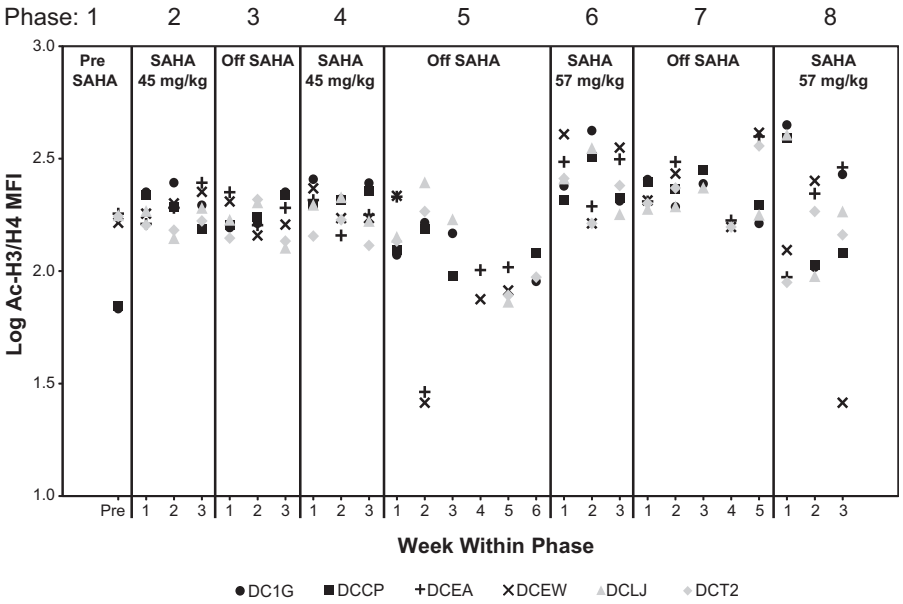

FIG 7 Acetylated histone levels in SAHA-treated cART-suppressed macaques. Shown are the longitudinal acetylated histone H3 and H4 levels in $CD4^+$ T cells measured by flow cytometry grouped into the 8 study phases indicated, with results for each animal represented by a unique plot symbol. Samples for analysis were collected at 2 h post-SAHA treatment for phases 2 and 4 and at 4 h post-SAHA treatment for phases 6 and 8.

DISCUSSION

A novel NHP model of cART-mediated suppression. We initiated these studies with two primary goals, the first of which was to develop and characterize a model of cART-mediated suppression in unselected SIVmac239-infected rhesus macaques of Indian origin, which constitutes one of the most widely used, best-characterized, authentic models of pathogenic HIV-1 infection. The second was to evaluate the activity of the HDACi SAHA in this model of cART-suppressed, SIV-infected macaques. Despite the utility of NHP models for investigating the complex *in vivo* biology of AIDS virus infection, their utilization for studies of suppressive cART, residual virus, and viral eradication/functional cure strategies has been limited, due at least in part to challenges with achieving sustained viral suppression to clinically relevant levels with available cART regimens in SIV-infected macaques (reviewed in reference 35). Previous studies suggested that typical three-drug ART regimens, like those used for HIV-1-infected humans, are often insufficient for durable suppression of SIVmac239 replication to clin-

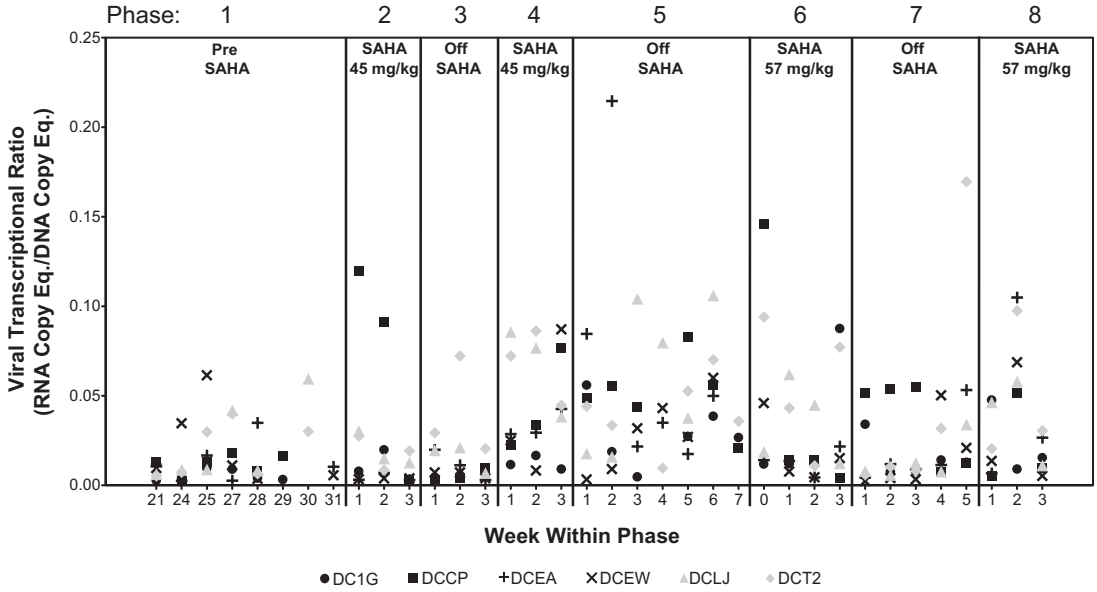

FIG 8 Viral transcriptional ratios in PBMC from SAHA-treated cART-suppressed macaques. Ratios of longitudinal cell-associated viral RNA and viral DNA levels in PBMC were measured by qRT-PCR and qPCR, respectively, and grouped into the 8 study phases indicated, with results for each animal represented by a unique plot symbol. Samples for analyses were collected at 2 h post-SAHA treatment for phases 2 and 4 and at 4 h post-SAHA treatment for phases 6 and 8.

ically relevant levels (i.e., <50 vRNA copies/ml), particularly for animals with high viral loads typical of SIVmac infection in Indian-origin rhesus macaques (35, 68–72). For the present study, we implemented a three-class (reverse transcriptase inhibitors, integrase strand transfer inhibitors, and protease inhibitors), six-drug regimen, which we identified through a number of pilot studies that evaluated various antiretroviral drugs in SIV-infected macaques (35; G. Q. Del Prete and J. D. Lifson, unpublished observations) and tested its efficacy in 6 *de novo* SIVmac239-infected animals. Although drug toxicities are a general concern for cART administration in NHPs, the need for prolonged treatment in a limited number of animals made it critical to utilize a drug regimen that was safe and well-tolerated. Importantly, no clinically significant adverse events were noted in any of the six treated animals with ~1 year of treatment. Modest changes in serum creatinine and inorganic phosphorous, consistent with mild tenofovir-related renal toxicity during prolonged administration in macaques, were measured in a subset of animals after ~10 to 12 months of cART (data not shown). Although the observed serum chemistry changes were minor, it may be possible to limit potential tenofovir-related renal toxicity in future studies through the utilization of tenofovir disoproxil fumarate (TDF), a prodrug form of tenofovir that may be effective at lower administered doses (Del Prete and Lifson, unpublished).

In addition to having an acceptable safety profile, the cART regimen effected impressive 4- to 5.5-log declines in plasma viral loads for all six animals (Fig. 2A), as well as declines in cell-associated viral RNA and DNA in PBMC, lymph nodes, and upper and lower gut-associated lymphoid tissues (Fig. 3). There was, however, a range in the absolute degree of suppression and in viral load nadirs among the animals, with three animals achieving stable plasma viral loads of <30 RNA copies/ml after ~6 months of treatment, two animals reaching plasma viral loads of <30 RNA copies/ml but with blips periodically exceeding 50 RNA copies/ml, and one animal with plasma viral loads that oscillated between <30 to over 100 RNA copies/ml (Fig. 2A and 6). Levels of persistent low-level viremia measured using ultrasensitive approaches in the best-suppressed animals at time points with viral loads below the standard assay's 30-copy/ml quantification limit were similar to levels of persistent low-level viremia reported for cART-suppressed humans (46, 73–76). The one animal that maintained the highest levels of plasma viremia on cART, animal DCEA, also possessed the highest pretreatment vRNA levels in LN and gut tissues, and these levels remained somewhat elevated on cART relative to the other treated animals (Fig. 3). In contrast, this animal's pretreatment PBMC-associated vRNA levels were the lowest among the six animals, and on cART its PBMC-associated vRNA levels were comparable to, or lower than, those in the other animals. Although this animal represents only one animal from a small cohort, this finding underscores the importance of examining tissues in addition to blood for studies of residual virus and highlights the value of the tissue accessibility afforded by animal models.

We initiated cART at 4 weeks postinfection, during the early chronic phase of infection. This time point was chosen to allow seeding of the residual viral reservoir while limiting the opportunity of the virus to develop and archive drug resistance variants, as has been shown for SHIVmne-infected animals prior to the initiation of ART (77) and may be more likely in the setting of the very high replication rates of SIVmac239. As shown in Fig. 2B, immune activation levels returned to approximate preinfection baseline levels with cART started at 4 weeks postinfection, in contrast to cART-suppressed humans, who typically begin therapy later in infection and maintain somewhat elevated levels of immune activation relative to levels in uninfected people (11, 54–56). Although this chronic immune activation is generally viewed as deleterious, it may in part reflect a functional antiviral immune response that contributes to cART-mediated suppression. Further evaluation of this and other treatment regimens will be required to refine the timing of cART initiation for optimal virologic suppression in SIV-infected NHPs.

Activity of SAHA in cART-suppressed SIV-infected macaques. Having established a cohort of SIVmac239-infected rhesus macaques with clinically relevant levels of cART-mediated suppression, our second primary study goal was to apply this model system to evaluate the impact of multiple administrations of the HDACi SAHA for safety and for activity on the residual virus pool in the setting of cART-mediated suppression. Consistent with recent and emerging findings in SAHA-treated cART-suppressed humans (30, 33, 41), we report here *in vivo* pharmacodynamic and virologic effects of SAHA treatment, including modulation of acetylated histone levels and disruption of the residual virus pool in treated animals, measured as statistically significant changes in the vRNA/vDNA ratio in PBMC. However, we also found that vRNA and vDNA, as well as *ex vivo*-inducible vRNA, were still detectable in all six study animals despite each receiving 84 doses of SAHA, suggesting that SAHA treatment alone in the setting of cART-mediated suppression may be insufficient for eradication of residual virus.

Prior to administering SAHA to our cART-suppressed animals, it was critical to first demonstrate clear pharmacodynamic and virologic effects of *ex vivo* SAHA treatment in SIV-infected rhesus $CD4^+$ T cells taken from cART-suppressed animals. As has been shown for human $CD4^+$ T cells taken from cART-suppressed patients, *ex vivo* SAHA treatment of $CD4^+$ T cells obtained from our cART-treated animals resulted in a clear increase in acetylated histone levels (H3 and H4), with associated increases in virus production over DMSO control-treated cells. The SAHA concentrations evaluated in these experiments were based on peak plasma SAHA levels, which reached >1.8 μM at 1 to 2 h postadministration, attained in a single-dose pharmacokinetic study in naive macaques (Fig. 4). However, the plasma SAHA concentrations measured in our treated animals at 2 and 4 h posttreatment for the 45-mg/kg and 57-mg/kg doses, respectively, were highly variable and substantially lower than those measured in the single-dose experiment (Table 1). Although the rapid pharmacokinetics of SAHA in plasma prevented an assessment of the peak levels attained in our cART-suppressed animals without multiple longitudinal postdose measurements, the presence of undigested food in the animals' stomachs, observed endoscopically at the plasma sampling time points (Del Prete and Lifson, unpublished), suggests that slower gastric emptying may have resulted in either delayed (78) or blunted peak plasma SAHA concentrations. Two key differences between the pharmacokinetic study and the suppressed animal study may have led to unexpected differences in gastric emptying and drug absorption. First, while animals in the pharmacokinetic study were fasted for 12 to 16 h prior to receiving SAHA in a food treat, the cART-suppressed animals had to consume daily SAHA as well as twice daily oral antiretroviral drugs ('812, '564, DRV, and RTV), precluding fasting prior to SAHA

treatment. Second, the single-dose pharmacokinetic study utilized restraint chair-trained animals that remained conscious for all sampling time points after SAHA administration, whereas the cART-suppressed animals were not restraint chair trained, requiring anesthetization prior to blood collection, which may have slowed digestive processes and drug absorption.

Despite potentially suboptimal SAHA dosing and/or sampling time points relative to dosing, we observed statistically significant, dose-dependent changes in acetylated histone levels associated with SAHA administration across all six study animals. Although peak plasma SAHA concentrations may have been lower in our suppressed, infected animals than the ~1 to 2 μM peak levels measured in singly dosed rhesus macaques (Fig. 4) and humans (30), the magnitudes of acetylated histone changes were comparable to those seen in single-dose SAHA-treated humans. Following a single dose of SAHA, total acetylated histone H3 levels measured by flow cytometry in eight treated humans showed a median increase of 1.6-fold (30). Similarly, in our six SAHA-treated animals, mean acetylated histone H3/H4 levels measured by flow cytometry during the SAHA treatment phases were 1.7- to 2.3-fold higher than those measured during the 6- to 7-week-long off-SAHA rest phase (phase 5).

Our studies revealed evidence for sustained modulation of histone acetylation after withdrawal of SAHA following prolonged administration. There was no statistically significant difference in Ac-H3/H4 levels between the two SAHA treatment phases at 45 mg/kg and the 3-week off-SAHA rest phase that separated them. In contrast, during the lengthier 6- to 7-week off-SAHA rest phase following the second course of SAHA at 45 mg/kg, there was a significant reduction in Ac-H3/H4 levels, suggesting that Ac-H3/H4 levels normalized with a longer off-treatment phase. At the higher dose of SAHA (57 mg/kg), we again observed sustained elevation of Ac-H3/H4 levels during the intervening off-SAHA rest phase, this time lasting 5 to 6 weeks, suggestive of potential dose dependence to the duration of sustained off-SAHA elevated acetylated histone levels. Importantly, although a significant increase in acetylated histone levels over pretreatment baselines could not be demonstrated during the first phase of SAHA treatment, perhaps due to the limited number of pretreatment data points and/or the lower dose of SAHA administered, Ac-H3/H4 levels during the 57-mg/kg SAHA administration portion of the study were significantly elevated over both the preceding rest phase and over the lower-dose SAHA treatment portion of the study. This finding suggests that the measured changes in acetylated histone levels were indeed induced by SAHA administration.

In addition to evidence for sustained histone modulation effects following multidose SAHA treatment, there was also evidence for potential development of refractoriness in responses after numerous high-dose treatments. A similar apparent refractoriness was observed in SAHA-treated humans when acetylated histone levels following 11 or 22 SAHA administrations were compared with acetylated histone levels following a single dose of SAHA in the same patient (33). Although in our study Ac-H3/H4 levels were highest for the final three study phases, encompassing both high-dose SAHA treatment courses, within these three phases there was a statistically significant downward trend over time in acetylated histone levels, with the lowest levels measured during the final on-SAHA phase. Dosing in the present study was based on clinical practice in oncology, where SAHA is given on a daily basis, to which we added off-treatment phases to assess the longitudinal dynamics of changes. Given the limited pharmacokinetic and pharmacodynamic data available for SAHA and other HDACi, further empirical studies will be required to determine the most effective dosing strategies for histone modulation patterns that result in the most robust virologic response. Accumulating data suggest that a more pulsatile mode of administration may be more effective (30, 33).

Although recruitment of histone deacetylases to the HIV LTR has been associated with viral latency (reviewed in references 24 and 26), the exact mechanisms underlying upregulation of viral transcription following HDACi treatment are not known (61). While a straightforward model involving direct modulation of histones at the viral LTR with subsequent increased chromatin accessibility and transcription has been proposed (25), the potential pleiotropic effects of cellular histone acetylation changes could result in multiple indirect mechanisms whereby viral expression may be modulated. In our SAHA-treated animals, statistically significant virologic changes, measured as changes in the ratio of vRNA to vDNA in PBMC, were identified during the SAHA treatment portion of the study, but they were not tightly linked to the specific on-SAHA/off-SAHA treatment phases. For example, no changes in the viral transcriptional ratio were observed through the first three study phases, which included the first SAHA treatment phase with a preceding pretreatment phase and a subsequent off-SAHA rest phase; however, a statistically significant increase in viral transcriptional ratio was measured during the second SAHA treatment phase. This result may reflect the complexities of histone modulation and cumulative downstream virologic effects in the setting of multiple daily HDACi treatments, with the first virologic measurements taken 7 days after the initiation of treatment. Alternatively, the apparent lack of an effect during the first SAHA treatment phase may reflect elevated pretreatment baselines that masked any transcriptional changes due to insufficient cART-mediated decay of productively infected cells at the start of the SAHA treatment portion of the study. Nevertheless, the viral transcriptional upregulation measured during study phases 4, 5, and 6 (>3-fold increases in mean levels over phases 1, 2, and 3) was similar in magnitude to the increase in viral RNA measured in resting $CD4^+$ T cells in SAHA-treated humans (30). Of note, these changes in cell-associated viral transcription were not associated with demonstrable increases in plasma viremia.

Previous *ex vivo* studies by Shan and coworkers (34) suggested that clearance of cells harboring reactivated latent proviruses may be unlikely in the absence of additional immune stimulation. Following the first course of SAHA at 57 mg/kg (phase 6), we observed a significant drop in the viral transcriptional ratio during the ensuing rest phase and the final high-dose SAHA treatment phase (phases 7 and 8). While this result may suggest apparent *in vivo* clearance of cells harboring SAHA-responsive proviruses—a finding that would have profound implications for HIV eradication/functional cure efforts—it may reflect, alternatively, the apparent refractory histone acetylation responses to prolonged SAHA treatment that were measured during the final two study phases. Efforts were made to quantify the fraction of $CD4^+$ T cells harboring SAHA-inducible proviruses at different study time points; however, the rarity of these cells and the limited survival bleed volumes obtainable from our animals precluded such quantitative analyses (data not shown). Although further investigation will be required to evaluate the fate of cells harboring inducible proviruses following *in vivo* HDACi treatment, previous studies

have shown that only a fraction of intact integrated proviruses in resting $CD4^+$ T cells from cART-suppressed individuals can be activated by HDACi. Indeed, even after 84 total doses of SAHA per animal, vRNA and vDNA were readily detected in blood and LN cells, and *ex vivo*-inducible SIV RNA could be readily detected in blood- and lymph node-derived $CD4^+$ T cells from all 6 animals, supporting the view that HDACi alone may be insufficient to achieve viral eradication.

Summary and implications. As seen in this study, the achievement of low, stable baseline viral loads is critical for evaluating the impact of therapies designed to induce limited numbers of rare targets. Although the cART regimen described here effected impressive levels of virologic suppression in both blood and tissues of all six treated animals, refinements to the cART regimen, including the timing of cART initiation, may improve upon the consistency and kinetics of suppression. The development and evaluation of alternate drug formulations, including coformulations to allow for multiple drug administrations in a single injection and delayed release formulations, along with incorporation of newer antiretrovirals, might allow for less frequent drug dosing and would improve the practical logistics of cART administration in NHPs (Del Prete and Lifson, unpublished). Similarly, refinements in the method and timing of HDACi administration, including exploration of more consistent administration routes and the use of alternative HDACi drugs, may result in more robust and consistent effects relative to timing of treatment and sampling. Despite some of the challenges discussed above, in cART-suppressed SIVmac239-infected Indian-origin rhesus macaques, this study showed *in vivo* pharmacodynamic and virologic effects of SAHA treatment similar to those seen in SAHA-treated cART-suppressed humans (30, 33, 41) and identified a number of previously unreported features of multidose SAHA treatment, including the capacity to perturb the residual virus pool and the potential for sustained modulation of histone acetylation following prolonged administration. This work establishes the feasibility, validity, and utility of cART-mediated suppression in one of the most widely used, authentically pathogenic animal models of AIDS for studies of residual virus and for the evaluation of strategies for functional cure or viral eradication.

ACKNOWLEDGMENTS

We thank the nonhuman primate care staff in the Laboratory Animal Sciences Program, Leidos Biomedical Research, Inc., for expert animal care. We are also grateful to Robert Papp, Sophie-Dorothee Clas, Helen Tanfara, Richard Desmangles, and Stephanie Allyn for conducting rhesus pharmacokinetic studies and data analyses, Marta Majdan for technical assistance for SAHA pharmacodynamic assessment in macaques, Deanne Rudd and Joan Ellis for assistance with plasma drug measurements, and Al Kane for assistance with preparation of figures. We also thank Romas Geleziunas at Gilead Biosciences for providing PMPA and FTC.

This work was supported in part with federal funds from the National Cancer Institute, National Institutes of Health, under contract number HHSN261200800001E.

C.M.T., R.I.S., D.J.H., and J.S.W. are current or former employees of Merck and Co. and may own Merck stock and/or stock options.

The content of this publication does not necessarily reflect the views or policies of the Department of Health and Human Services, nor does mention of trade names, commercial products, or organizations imply endorsement by the U.S. government.

REFERENCES

1. **Chun TW, Justement JS, Murray D, Hallahan CW, Maenza J, Collier AC, Sheth PM, Kaul R, Ostrowski M, Moir S, Kovacs C, Fauci AS.** 2010. Rebound of plasma viremia following cessation of antiretroviral therapy despite profoundly low levels of HIV reservoir: implications for eradication. AIDS **24:**2803–2808. http://dx.doi.org/10.1097/QAD.0b013e328340a239.
2. **Davey RT, Jr, Bhat N, Yoder C, Chun TW, Metcalf JA, Dewar R, Natarajan V, Lempicki RA, Adelsberger JW, Miller KD, Kovacs JA, Polis MA, Walker RE, Falloon J, Masur H, Gee D, Baseler M, Dimitrov DS, Fauci AS, Lane HC.** 1999. HIV-1 and T cell dynamics after interruption of highly active antiretroviral therapy (HAART) in patients with a history of sustained viral suppression. Proc. Natl. Acad. Sci. U. S. A. **96:**15109–15114. http://dx.doi.org/10.1073/pnas.96.26.15109.
3. **Chun TW, Carruth L, Finzi D, Shen X, DiGiuseppe JA, Taylor H, Hermankova M, Chadwick K, Margolick J, Quinn TC, Kuo YH, Brookmeyer R, Zeiger MA, Barditch-Crovo P, Siliciano RF.** 1997. Quantification of latent tissue reservoirs and total body viral load in HIV-1 infection. Nature **387:**183–188. http://dx.doi.org/10.1038/387183a0.
4. **Chun TW, Finzi D, Margolick J, Chadwick K, Schwartz D, Siliciano RF.** 1995. In vivo fate of HIV-1-infected T cells: quantitative analysis of the transition to stable latency. Nat. Med. **1:**1284–1290. http://dx.doi.org/10.1038/nm1295-1284.
5. **Finzi D, Blankson J, Siliciano JD, Margolick JB, Chadwick K, Pierson T, Smith K, Lisziewicz J, Lori F, Flexner C, Quinn TC, Chaisson RE, Rosenberg E, Walker B, Gange S, Gallant J, Siliciano RF.** 1999. Latent infection of $CD4^+$ T cells provides a mechanism for lifelong persistence of HIV-1, even in patients on effective combination therapy. Nat. Med. **5:**512–517. http://dx.doi.org/10.1038/8394.
6. **Wang F, Flanagan J, Su N, Wang LC, Bui S, Nielson A, Wu X, Vo HT, Ma XJ, Luo Y.** 2012. RNAscope: a novel in situ RNA analysis platform for formalin-fixed, paraffin-embedded tissues. J. Mol. Diagn. **14:**22–29. http://dx.doi.org/10.1016/j.jmoldx.2011.08.002.
7. **Antiretroviral Therapy Cohort Collaboration.** 2008. Life expectancy of individuals on combination antiretroviral therapy in high-income countries: a collaborative analysis of 14 cohort studies. Lancet **372:**293–299. http://dx.doi.org/10.1016/S0140-6736(08)61113-7.
8. **Bhaskaran K, Hamouda O, Sannes M, Boufassa F, Johnson AM, Lambert PC, Porter K.** 2008. Changes in the risk of death after HIV seroconversion compared with mortality in the general population. JAMA **300:**51–59. http://dx.doi.org/10.1001/jama.300.1.51.
9. **Lohse N, Hansen AB, Pedersen G, Kronborg G, Gerstoft J, Sorensen HT, Vaeth M, Obel N.** 2007. Survival of persons with and without HIV infection in Denmark, 1995-2005. Ann. Intern. Med. **146:**87–95. http://dx.doi.org/10.7326/0003-4819-146-2-200701160-00003.
10. **Losina E, Schackman BR, Sadownik SN, Gebo KA, Walensky RP, Chiosi JJ, Weinstein MC, Hicks PL, Aaronson WH, Moore RD, Paltiel AD, Freedberg KA.** 2009. Racial and sex disparities in life expectancy losses among HIV-infected persons in the United States: impact of risk behavior, late initiation, and early discontinuation of antiretroviral therapy. Clin. Infect. Dis. **49:**1570–1578. http://dx.doi.org/10.1086/644772.
11. **Hunt PW, Martin JN, Sinclair E, Bredt B, Hagos E, Lampiris H, Deeks SG.** 2003. T cell activation is associated with lower $CD4^+$ T cell gains in human immunodeficiency virus-infected patients with sustained viral suppression during antiretroviral therapy. J. Infect. Dis. **187:**1534–1543. http://dx.doi.org/10.1086/374786.
12. **Valdez H, Connick E, Smith KY, Lederman MM, Bosch RJ, Kim RS, St Clair M, Kuritzkes DR, Kessler H, Fox L, Blanchard-Vargas M, Landay A.** 2002. Limited immune restoration after 3 years' suppression of HIV-1 replication in patients with moderately advanced disease. AIDS **16:**1859–1866. http://dx.doi.org/10.1097/00002030-200209270-00002.
13. **Massanella M, Negredo E, Perez-Alvarez N, Puig J, Ruiz-Hernandez R, Bofill M, Clotet B, Blanco J.** 2010. CD4 T-cell hyperactivation and susceptibility to cell death determine poor CD4 T-cell recovery during suppressive HAART. AIDS **24:**959–968. http://dx.doi.org/10.1097/QAD.0b013e328337b957.
14. **Neuhaus J, Jacobs DR, Jr, Baker JV, Calmy A, Duprez D, La Rosa A, Kuller LH, Pett SL, Ristola M, Ross MJ, Shlipak MG, Tracy R, Neaton JD.** 2010. Markers of inflammation, coagulation, and renal function are elevated in adults with HIV infection. J. Infect. Dis. **201:**1788–1795. http://dx.doi.org/10.1086/652749.
15. **Lederman MM, Calabrese L, Funderburg NT, Clagett B, Medvik K,**

Bonilla H, Gripshover B, Salata RA, Taege A, Lisgaris M, McComsey GA, Kirchner E, Baum J, Shive C, Asaad R, Kalayjian RC, Sieg SF, Rodriguez B. 2011. Immunologic failure despite suppressive antiretroviral therapy is related to activation and turnover of memory CD4 cells. J. Infect. Dis. **204:**1217–1226. http://dx.doi.org/10.1093/infdis/jir507.

16. **Jain V, Hartogensis W, Bacchetti P, Hunt PW, Hatano H, Sinclair E, Epling L, Lee TH, Busch MP, McCune JM, Pilcher CD, Hecht FM, Deeks SG.** 2013. Antiretroviral therapy initiated within 6 months of HIV infection is associated with lower T-cell activation and smaller HIV reservoir size. J. Infect. Dis. **208:**1202–1211. http://dx.doi.org/10.1093/infdis/jit311.
17. **Vinikoor MJ, Cope A, Gay CL, Ferrari G, McGee KS, Kuruc JD, Lennox JL, Margolis DM, Hicks CB, Eron JJ.** 2013. Antiretroviral therapy initiated during acute HIV infection fails to prevent persistent T-cell activation. J. Acquir. Immune Defic. Syndr. **62:**505–508. http://dx.doi.org/10.1097/QAI.0b013e318285cd33.
18. **Wong JK, Hezareh M, Gunthard HF, Havlir DV, Ignacio CC, Spina CA, Richman DD.** 1997. Recovery of replication-competent HIV despite prolonged suppression of plasma viremia. Science **278:**1291–1295. http://dx.doi.org/10.1126/science.278.5341.1291.
19. **Gras G, Kaul M.** 2010. Molecular mechanisms of neuroinvasion by monocytes-macrophages in HIV-1 infection. Retrovirology **7:**30. http://dx.doi.org/10.1186/1742-4690-7-30.
20. **Carter CC, Onafuwa-Nuga A, McNamara LA, Riddell J, IV, Bixby D, Savona MR, Collins KL.** 2010. HIV-1 infects multipotent progenitor cells causing cell death and establishing latent cellular reservoirs. Nat. Med. **16:**446–451. http://dx.doi.org/10.1038/nm.2109.
21. **Clements JE, Li M, Gama L, Bullock B, Carruth LM, Mankowski JL, Zink MC.** 2005. The central nervous system is a viral reservoir in simian immunodeficiency virus-infected macaques on combined antiretroviral therapy: a model for human immunodeficiency virus patients on highly active antiretroviral therapy. J. Neurovirol. **11:**180–189. http://dx.doi.org/10.1080/13550280590922748-1.
22. **Dinoso JB, Rabi SA, Blankson JN, Gama L, Mankowski JL, Siliciano RF, Zink MC, Clements JE.** 2009. A simian immunodeficiency virus-infected macaque model to study viral reservoirs that persist during highly active antiretroviral therapy. J. Virol. **83:**9247–9257. http://dx.doi.org/10.1128/JVI.00840-09.
23. **Fletcher CV, Staskus K, Wietgrefe SW, Rothenberger M, Reilly C, Chipman JG, Beilman GJ, Khoruts A, Thorkelson A, Schmidt TE, Anderson J, Perkey K, Stevenson M, Perelson AS, Douek DC, Haase AT, Schacker TW.** 2014. Persistent HIV-1 replication is associated with lower antiretroviral drug concentrations in lymphatic tissues. Proc. Natl. Acad. Sci. U. S. A. **111:**2307–2312. http://dx.doi.org/10.1073/pnas.1318249111.
24. **Williams SA, Greene WC.** 2007. Regulation of HIV-1 latency by T-cell activation. Cytokine **39:**63–74. http://dx.doi.org/10.1016/j.cyto.2007.05.017.
25. **Richman DD, Margolis DM, Delaney M, Greene WC, Hazuda D, Pomerantz RJ.** 2009. The challenge of finding a cure for HIV infection. Science **323:**1304–1307. http://dx.doi.org/10.1126/science.1165706.
26. **Mbonye U, Karn J.** 2014. Transcriptional control of HIV latency: cellular signaling pathways, epigenetics, happenstance and the hope for a cure. Virology **454-455:**328–329. http://dx.doi.org/10.1016/j.virol.2014.02.008.
27. **Ylisastigui L, Archin NM, Lehrman G, Bosch RJ, Margolis DM.** 2004. Coaxing HIV-1 from resting CD4 T cells: histone deacetylase inhibition allows latent viral expression. AIDS **18:**1101–1108. http://dx.doi.org/10.1097/00002030-200405210-00003.
28. **Archin NM, Espeseth A, Parker D, Cheema M, Hazuda D, Margolis DM.** 2009. Expression of latent HIV induced by the potent HDAC inhibitor suberoylanilide hydroxamic acid. AIDS Res. Hum. Retroviruses **25:**207–212. http://dx.doi.org/10.1089/aid.2008.0191.
29. **Archin NM, Keedy KS, Espeseth A, Dang H, Hazuda DJ, Margolis DM.** 2009. Expression of latent human immunodeficiency type 1 is induced by novel and selective histone deacetylase inhibitors. AIDS **23:**1799–1806. http://dx.doi.org/10.1097/QAD.0b013e32832ec1dc.
30. **Archin NM, Liberty AL, Kashuba AD, Choudhary SK, Kuruc JD, Crooks AM, Parker DC, Anderson EM, Kearney MF, Strain MC, Richman DD, Hudgens MG, Bosch RJ, Coffin JM, Eron JJ, Hazuda DJ, Margolis DM.** 2012. Administration of vorinostat disrupts HIV-1 latency in patients on antiretroviral therapy. Nature **487:**482–485. http://dx.doi.org/10.1038/nature11286.
31. **Contreras X, Schweneker M, Chen CS, McCune JM, Deeks SG, Martin J, Peterlin BM.** 2009. Suberoylanilide hydroxamic acid reactivates HIV from latently infected cells. J. Biol. Chem. **284:**6782–6789. http://dx.doi.org/10.1074/jbc.M807898200.
32. **Ylisastigui L, Coull JJ, Rucker VC, Melander C, Bosch RJ, Brodie SJ, Corey L, Sodora DL, Dervan PB, Margolis DM.** 2004. Polyamides reveal a role for repression in latency within resting T cells of HIV-infected donors. J. Infect. Dis. **190:**1429–1437. http://dx.doi.org/10.1086/423822.
33. **Archin NM, Bateson R, Tripathy M, Crooks AM, Yang KH, Dahl NP, Kearney MF, Anderson EM, Coffin JM, Strain MC, Richman DD, Robertson KR, Kashuba AD, Bosch RJ, Hazuda DJ, Kuruc JD, Eron JJ, Margolis DM.** 2014. HIV-1 expression within resting CD4 T-cells following multiple doses of Vorinostat. J. Infect. Dis. **210:**728–735. http://dx.doi.org/10.1093/infdis/jiu155.
34. **Shan L, Deng K, Shroff NS, Durand CM, Rabi SA, Yang HC, Zhang H, Margolick JB, Blankson JN, Siliciano RF.** 2012. Stimulation of HIV-1-specific cytolytic T lymphocytes facilitates elimination of latent viral reservoir after virus reactivation. Immunity **36:**491–501. http://dx.doi.org/10.1016/j.immuni.2012.01.014.
35. **Del Prete GQ, Lifson JD.** 2013. Considerations in the development of nonhuman primate models of combination antiretroviral therapy for studies of AIDS virus suppression, residual virus, and curative strategies. Curr. Opin. HIV AIDS **8:**262–272. http://dx.doi.org/10.1097/COH.0b013e328361cf40.
36. **Whetter LE, Ojukwu IC, Novembre FJ, Dewhurst S.** 1999. Pathogenesis of simian immunodeficiency virus infection. J. Gen. Virol. **80:**1557–1568.
37. **Del Prete GQ, Scarlotta M, Newman L, Reid C, Parodi LM, Roser JD, Oswald K, Marx PA, Miller CJ, Desrosiers RC, Barouch DH, Pal R, Piatak M, Jr, Chertova E, Giavedoni LD, O'Connor DH, Lifson JD, Keele BF.** 2013. Comparative characterization of transfection- and infection-derived simian immunodeficiency virus challenge stocks for in vivo nonhuman primate studies. J. Virol. **87:**4584–4595. http://dx.doi.org/10.1128/JVI.03507-12.
38. **Keele BF, Li H, Learn GH, Hraber P, Giorgi EE, Grayson T, Sun C, Chen Y, Yeh WW, Letvin NL, Mascola JR, Nabel GJ, Haynes BF, Bhattacharya T, Perelson AS, Korber BT, Hahn BH, Shaw GM.** 2009. Low-dose rectal inoculation of rhesus macaques by SIVsmE660 or SIVmac251 recapitulates human mucosal infection by HIV-1. J. Exp. Med. **206:**1117–1134. http://dx.doi.org/10.1084/jem.20082831.
39. **Strickland SL, Gray RR, Lamers SL, Burdo TH, Huenink E, Nolan DJ, Nowlin B, Alvarez X, Midkiff CC, Goodenow MM, Williams K, Salemi M.** 2011. Significant genetic heterogeneity of the SIVmac251 viral swarm derived from different sources. AIDS Res. Hum. Retroviruses **27:**1327–1332. http://dx.doi.org/10.1089/aid.2011.0100.
40. **Bixby JG, Laur O, Johnson WE, Desrosiers RC.** 2010. Diversity of envelope genes from an uncloned stock of SIVmac251. AIDS Res. Hum. Retroviruses **26:**1115–1131. http://dx.doi.org/10.1089/aid.2010.0029.
41. **Elliot J, Solomon A, Smith M, Palmer S, Prince M, Watson J, Hoy J, McMahon J, Lewin SR.** 2013. The safety and effect of multiple doses of vorinostat on HIV transcription in HIV^+ patients receiving cART, abstr 50LB Final Program 20th Conference on Retroviruses and Opportunistic Infections, Atanta, GACROI, San Francisco, CA.
42. **Lifson JD, Piatak M, Jr, Cline AN, Rossio JL, Purcell J, Pandrea I, Bischofberger N, Blanchard J, Veazey RS.** 2003. Transient early post-inoculation anti-retroviral treatment facilitates controlled infection with sparing of $CD4^+$ T cells in gut-associated lymphoid tissues in SIVmac239-infected rhesus macaques, but not resistance to rechallenge. J. Med. Primatol. **32:**201–210. http://dx.doi.org/10.1034/j.1600-0684.2003.00026.x.
43. **Suryanarayana K, Wiltrout TA, Vasquez GM, Hirsch VM, Lifson JD.** 1998. Plasma SIV RNA viral load determination by real-time quantification of product generation in reverse transcriptase-polymerase chain reaction. AIDS Res. Hum. Retroviruses **14:**183–189. http://dx.doi.org/10.1089/aid.1998.14.183.
44. **Cline AN, Bess JW, Piatak M, Jr, Lifson JD.** 2005. Highly sensitive SIV plasma viral load assay: practical considerations, realistic performance expectations, and application to reverse engineering of vaccines for AIDS. J. Med. Primatol. **34:**303–312. http://dx.doi.org/10.1111/j.1600-0684.2005.00128.x.
45. **Hughes SH, Greenhouse JJ, Petropoulos CJ, Sutrave P.** 1987. Adaptor plasmids simplify the insertion of foreign DNA into helper-independent retroviral vectors. J. Virol. **61:**3004–3012.
46. **Palmer S, Wiegand AP, Maldarelli F, Bazmi H, Mican JM, Polis M, Dewar RL, Planta A, Liu S, Metcalf JA, Mellors JW, Coffin JM.** 2003.

New real-time reverse transcriptase-initiated PCR assay with single-copy sensitivity for human immunodeficiency virus type 1 RNA in plasma. J. Clin. Microbiol. **41:**4531–4536. http://dx.doi.org/10.1128/JCM.41.10.4531-4536.2003.

47. **Hansen SG, Ford JC, Lewis MS, Ventura AB, Hughes CM, Coyne-Johnson L, Whizin N, Oswald K, Shoemaker R, Swanson T, Legasse AW, Chiuchiolo MJ, Parks CL, Axthelm MK, Nelson JA, Jarvis MA, Piatak M, Jr, Lifson JD, Picker LJ.** 2011. Profound early control of highly pathogenic SIV by an effector memory T-cell vaccine. Nature **473:**523–527. http://dx.doi.org/10.1038/nature10003.
48. **Del Prete GQ, Kearney MF, Spindler J, Wiegand A, Chertova E, Roser JD, Estes JD, Hao XP, Trubey CM, Lara A, Lee K, Chaipan C, Bess JW, Jr, Nagashima K, Keele BF, Macallister R, Smedley J, Pathak VK, Kewalramani VN, Coffin JM, Lifson JD.** 2012. Restricted replication of xenotropic murine leukemia virus-related virus in pigtailed macaques. J. Virol. **86:**3152–3166. http://dx.doi.org/10.1128/JVI.06886-11.
49. **Tabb B, Morcock DR, Trubey CM, Quinones OA, Hao XP, Smedley J, Macallister R, Piatak M, Jr, Harris LD, Paiardini M, Silvestri G, Brenchley JM, Alvord WG, Lifson JD, Estes JD.** 2013. Reduced inflammation and lymphoid tissue immunopathology in rhesus macaques receiving anti-tumor necrosis factor treatment during primary simian immunodeficiency virus infection. J. Infect. Dis. **207:**880–892. http://dx.doi.org/10.1093/infdis/jis643.
50. **Crowder MJ, Hand DJ.** 1990. Analysis of repeated measures, p 27–42. Chapman and Hall, London, United Kingdom.
51. **Pinheiro JC, Bates DM.** 2000. Mixed-effects models in S and S-Plus. Springer-Verlag, New York, NY.
52. **Benjamini Y, Hochberg Y.** 1995. Controlling the false discovery rate: a practical and powerful approach to multiple testing. J. R. Stat. Soc. B Stat. Methodol. **57:**289–300.
53. **Van Rompay KK, Durand-Gasselin L, Brignolo LL, Ray AS, Abel K, Cihlar T, Spinner A, Jerome C, Moore J, Kearney BP, Marthas ML, Reiser H, Bischofberger N.** 2008. Chronic administration of tenofovir to rhesus macaques from infancy through adulthood and pregnancy: summary of pharmacokinetics and biological and virological effects. Antimicrob. Agents Chemother. **52:**3144–3160. http://dx.doi.org/10.1128/AAC.00350-08.
54. **Gray CM, Schapiro JM, Winters MA, Merigan TC.** 1998. Changes in $CD4^+$ and $CD8^+$ T cell subsets in response to highly active antiretroviral therapy in HIV type 1-infected patients with prior protease inhibitor experience. AIDS Res. Hum. Retroviruses **14:**561–569. http://dx.doi.org/10.1089/aid.1998.14.561.
55. **French MA, King MS, Tschampa JM, da Silva BA, Landay AL.** 2009. Serum immune activation markers are persistently increased in patients with HIV infection after 6 years of antiretroviral therapy despite suppression of viral replication and reconstitution of $CD4^+$ T cells. J. Infect. Dis. **200:**1212–1215. http://dx.doi.org/10.1086/605890.
56. **Kolber MA, Saenz MO, Tanner TJ, Arheart KL, Pahwa S, Liu H.** 2008. Intensification of a suppressive HAART regimen increases CD4 counts and decreases $CD8^+$ T-cell activation. Clin. Immunol. **126:**315–321. http://dx.doi.org/10.1016/j.clim.2007.10.002.
57. **Kaur A, Hale CL, Ramanujan S, Jain RK, Johnson RP.** 2000. Differential dynamics of $CD4^+$ and $CD8^+$ T-lymphocyte proliferation and activation in acute simian immunodeficiency virus infection. J. Virol. **74:**8413–8424. http://dx.doi.org/10.1128/JVI.74.18.8413-8424.2000.
58. **Quivy V, Adam E, Collette Y, Demonte D, Chariot A, Vanhulle C, Berkhout B, Castellano R, de Launoit Y, Burny A, Piette J, Bours V, Van Lint C.** 2002. Synergistic activation of human immunodeficiency virus type 1 promoter activity by NF-κB and inhibitors of deacetylases: potential perspectives for the development of therapeutic strategies. J. Virol. **76:**11091–11103. http://dx.doi.org/10.1128/JVI.76.21.11091-11103.2002.
59. **Van Lint C, Emiliani S, Ott M, Verdin E.** 1996. Transcriptional activation and chromatin remodeling of the HIV-1 promoter in response to histone acetylation. EMBO J. **15:**1112–1120.
60. **Reuse S, Calao M, Kabeya K, Guiguen A, Gatot JS, Quivy V, Vanhulle C, Lamine A, Vaira D, Demonte D, Martinelli V, Veithen E, Cherrier T, Avettand V, Poutrel S, Piette J, de Launoit Y, Moutschen M, Burny A, Rouzioux C, De Wit S, Herbein G, Rohr O, Collette Y, Lambotte O, Clumeck N, Van Lint C.** 2009. Synergistic activation of HIV-1 expression by deacetylase inhibitors and prostratin: implications for treatment of latent infection. PLoS One **4:**e6093. http://dx.doi.org/10.1371/journal.pone.0006093.
61. **Bartholomeeusen K, Fujinaga K, Xiang Y, Peterlin BM.** 2013. Histone deacetylase inhibitors (HDACis) that release the positive transcription elongation factor b (P-TEFb) from its inhibitory complex also activate HIV transcription. J. Biol. Chem. **288:**14400–14407. http://dx.doi.org/10.1074/jbc.M113.464834.
62. **Wightman F, Lu HK, Solomon AE, Saleh S, Harman AN, Cunningham AL, Gray L, Churchill M, Cameron PU, Dear AE, Lewin SR.** 2013. Entinostat is a histone deacetylase inhibitor selective for class 1 histone deacetylases and activates HIV production from latently infected primary T cells. AIDS **27:**2853–2862. http://dx.doi.org/10.1097/QAD.0000000000000067.
63. **Edelstein LC, Micheva-Viteva S, Phelan BD, Dougherty JP.** 2009. Short communication: activation of latent HIV type 1 gene expression by suberoylanilide hydroxamic acid (SAHA), an HDAC inhibitor approved for use to treat cutaneous T cell lymphoma. AIDS Res. Hum. Retroviruses **25:**883–887. http://dx.doi.org/10.1089/aid.2008.0294.
64. **Matalon S, Palmer BE, Nold MF, Furlan A, Kassu A, Fossati G, Mascagni P, Dinarello CA.** 2010. The histone deacetylase inhibitor ITF2357 decreases surface CXCR4 and CCR5 expression on $CD4^+$ T-cells and monocytes and is superior to valproic acid for latent HIV-1 expression in vitro. J. Acquir. Immune Defic. Syndr. **54:**1–9. http://dx.doi.org/10.1097/QAI.0b013e3181d3dca3.
65. **Ying H, Zhang Y, Lin S, Han Y, Zhu HZ.** 2010. Histone deacetylase inhibitor Scriptaid reactivates latent HIV-1 promoter by inducing histone modification in in vitro latency cell lines. Int. J. Mol. Med. **26:**265–272. http://dx.doi.org/10.3892/ijmm_00000461.
66. **Cillo AR, Sobolewski MD, Bosch RJ, Fyne E, Piatak M, Jr, Coffin JM, Mellors JW.** 2014. Quantification of HIV-1 latency reversal in resting $CD4^+$ T cells from patients on suppressive antiretroviral therapy. Proc. Natl. Acad. Sci. U. S. A. **111:**7078–7083. http://dx.doi.org/10.1073/pnas.1402873111.
67. **Mohammadi P, di Iulio J, Munoz M, Martinez R, Bartha I, Cavassini M, Thorball C, Fellay J, Beerenwinkel N, Ciuffi A, Telenti A.** 2014. Dynamics of HIV latency and reactivation in a primary $CD4^+$ T cell model. PLoS Pathog. **10:**e1004156. http://dx.doi.org/10.1371/journal.ppat.1004156.
68. **Demberg T, Brocca-Cofano E, Xiao P, Venzon D, Vargas-Inchaustegui D, Lee EM, Kalisz I, Kalyanaraman VS, Dipasquale J, McKinnon K, Robert-Guroff M.** 2012. Dynamics of memory B-cell populations in blood, lymph nodes, and bone marrow during antiretroviral therapy and envelope boosting in simian immunodeficiency virus SIVmac251-infected rhesus macaques. J. Virol. **86:**12591–12604. http://dx.doi.org/10.1128/JVI.00298-12.
69. **Horiike M, Iwami S, Kodama M, Sato A, Watanabe Y, Yasui M, Ishida Y, Kobayashi T, Miura T, Igarashi T.** 2012. Lymph nodes harbor viral reservoirs that cause rebound of plasma viremia in SIV-infected macaques upon cessation of combined antiretroviral therapy. Virology **423:**107–118. http://dx.doi.org/10.1016/j.virol.2011.11.024.
70. **Lugli E, Mueller YM, Lewis MG, Villinger F, Katsikis PD, Roederer M.** 2011. IL-15 delays suppression and fails to promote immune reconstitution in virally suppressed chronically SIV-infected macaques. Blood **118:**2520–2529. http://dx.doi.org/10.1182/blood-2011-05-351155.
71. **Shytaj IL, Norelli S, Chirullo B, Della Corte A, Collins M, Yalley-Ogunro J, Greenhouse J, Iraci N, Acosta EP, Barreca ML, Lewis MG, Savarino A.** 2012. A highly intensified ART regimen induces long-term viral suppression and restriction of the viral reservoir in a simian AIDS model. PLoS Pathog. **8:**e1002774. http://dx.doi.org/10.1371/journal.ppat.1002774.
72. **zur Megede J, Sanders-Beer B, Silvera P, Golightly D, Bowlsbey A, Hebblewaite D, Sites D, Nieves-Duran L, Srivastava R, Otten GR, Rabussay D, Zhang L, Ulmer JB, Barnett SW, Donnelly JJ.** 2008. A therapeutic SIV DNA vaccine elicits T-cell immune responses, but no sustained control of viremia in SIVmac239-infected rhesus macaques. AIDS Res. Hum. Retroviruses **24:**1103–1116. http://dx.doi.org/10.1089/aid.2008.0055.
73. **Maldarelli F, Palmer S, King MS, Wiegand A, Polis MA, Mican J, Kovacs JA, Davey RT, Rock-Kress D, Dewar R, Liu S, Metcalf JA, Rehm C, Brun SC, Hanna GJ, Kempf DJ, Coffin JM, Mellors JW.** 2007. ART suppresses plasma HIV-1 RNA to a stable set point predicted by pretherapy viremia. PLoS Pathog. **3:**e46. http://dx.doi.org/10.1371/journal.ppat.0030046.
74. **Dornadula G, Zhang H, VanUitert B, Stern J, Livornese L, Jr, Ingerman MJ, Witek J, Kedanis RJ, Natkin J, DeSimone J, Pomerantz RJ.** 1999. Residual HIV-1 RNA in blood plasma of patients taking suppressive

highly active antiretroviral therapy. JAMA **282:**1627–1632. http://dx.doi.org/10.1001/jama.282.17.1627.

75. **Fischer M, Gunthard HF, Opravil M, Joos B, Huber W, Bisset LR, Ott P, Boni J, Weber R, Cone RW.** 2000. Residual HIV-RNA levels persist for up to 2.5 years in peripheral blood mononuclear cells of patients on potent antiretroviral therapy. AIDS Res. Hum. Retroviruses **16:**1135–1140. http://dx.doi.org/10.1089/088922200414974.
76. **Palmer S, Maldarelli F, Wiegand A, Bernstein B, Hanna GJ, Brun SC, Kempf DJ, Mellors JW, Coffin JM, King MS.** 2008. Low-level viremia persists for at least 7 years in patients on suppressive antiretroviral therapy. Proc. Natl. Acad. Sci. U. S. A. **105:**3879–3884. http://dx.doi.org/10.1073/pnas.0800050105.
77. **Boltz VF, Ambrose Z, Kearney MF, Shao W, Kewalramani VN, Maldarelli F, Mellors JW, Coffin JM.** 2012. Ultrasensitive allele-specific PCR reveals rare preexisting drug-resistant variants and a large replicating virus population in macaques infected with a simian immunodeficiency virus containing human immunodeficiency virus reverse transcriptase. J. Virol. **86:**12525–12530. http://dx.doi.org/10.1128/JVI.01963-12.
78. **Rubin EH, Agrawal NG, Friedman EJ, Scott P, Mazina KE, Sun L, Du L, Ricker JL, Frankel SR, Gottesdiener KM, Wagner JA, Iwamoto M.** 2006. A study to determine the effects of food and multiple dosing on the pharmacokinetics of vorinostat given orally to patients with advanced cancer. Clin. Cancer Res. **12:**7039–7045. http://dx.doi.org/10.1158/1078-0432.CCR-06-1802.